Functional analysis of MIKC^{C}-type MADS-box genes in the moss *Physcomitrella patens* to infer the functional evolution of the gene family

KOSHIMIZU SHIZUKA

Doctor of Philosophy

Department of Basic Biology
School of Life Science
SOKENDAI (The Graduate University for Advanced Studies)

Functional analysis of MIKC^{C}-type MADS-box genes in the moss *Physcomitrella patens* to infer the functional evolution of the gene family

ヒメツリガネゴケにおける MIKC^{C} タイプ MADS-box 遺伝子の機能解析および同遺伝子族の機能進化の推定

Koshimizu, Shizuka

越水　静

Doctor of Philosophy

Department of Basic Biology
School of Life Science
SOKENDAI
(The Graduate University for Advanced Studies)

2017

Table of contents

1. General introduction 3

2. Introduction 6

3. Materials and Methods 8
   3.1. Plant materials and culture conditions 8
   3.2. Transformation 8
   3.3. DNA gel blot analysis 19
   3.4. Microscopy analysis 19
   3.5. Protein expression using the oestrogen inducing system 20
   3.6. Quantitative RT-PCR analysis 20
   3.7. Transcriptome analyses 20
   3.8. Observation by TEM 21
   3.9. Extracellular lipid identification and quantification 22
   3.10. Reactivation experiment for sperm 23

4. Results 25
   4.1. Localization of MIKC^{C}-type MADS-domain proteins fused with reporter proteins 25
   4.2. MIKC^{C}-type MADS-box genes negatively regulate cell divisions and growth in the gametophore stem 31
   4.3. External water conduction is defective in the deletion mutant lines 38
   4.4. Sperm entry into archegonia is less efficient in the deletion mutant lines 45
   4.5. MIKC^{C}-type MADS-box proteins regulate genes involved in flagellum formation 47

5. Discussion 59

6. General discussion 64

7. Acknowledgements 67

8. References 68

1. General introduction

MADS-domain proteins are transcription factors found in wide range of eukaryotes including green plants, metazoans, and fungi, and the domain sequences are conserved between them (Yanofsky et al., 1990; Schwarz-sommer et al., 1990). MADS-domain protein family can be classified into two types, type I and II, by their domain structures. In green plants, type I MADS-domain proteins have only a MADS domain, which consists of about 60 amino acid residues with DNA binding activity (De Bodt et al., 2003; Kofuji et al., 2003; Parenicova, 2003). In contrast, type II MADS-domain proteins have I, K, and C domains in addition to the MADS domain. I domain influences specificity in the formation of DNA binding dimers and K domain contributes to heterodimerization and higher-order complex formation. C domain is postulated to have variable roles as the determinant of functional and protein-interaction specificity (Kaufmann et al., 2005). Because of this domain structure, type II MADS-domain proteins are called MIKC-type. MIKC-type MADS-domain proteins can be further classified into classic ($MIKC^C$) or star (MIKC*) type by length of I domain or duplication of a part of K domain (Henschel et al., 2002; Kwantes et al., 2012). $MIKC^C$-type MADS-domain proteins include key regulators of flowering and homeotic selectors for floral organs in angiosperms through the interaction with different sets of other MADS-domain proteins, other transcription factors, or chromatin remodeling factors (Smaczniak et al., 2012b; Wu et al., 2012). The various protein interactions enable $MIKC^C$-type proteins to regulate different sets of genes, including those encoding proteins involved in flowering, determination of floral organ identity, hormone biosynthesis, signalling, and growth regulation (Dornelas et al., 2011; Ito, 2011). As a result, $MIKC^C$-type MADS-domain proteins function in a range of

developmental processes in gametophytes, seeds, embryos, roots, leaves, inflorescences, and fruits (Smaczniak et al., 2012a).

Genes encoding MADS-domain proteins are called as MADS-box genes. Approximately 40 MIKC^{C}-type MADS-box genes are present in angiosperm species. In contrast, single MIKC^{C}-type MADS-box genes have been found in species of the Zygnematophyceae, Charales, and Coleochaetales algae (Tanabe et al., 2005), which are inferred to be closely related lineages to extant land plants (Wickett et al., 2014). The moss *Physcomitrella patens* is a member of a basal lineage of land plants, and possesses six MIKC^{C}-type MADS-box genes (Rensing et al., 2008), which diverged in the moss lineage (Barker and Ashton, 2013). These results suggest that the common ancestor of land plants had a single MIKC^{C}-type MADS-box gene, and that the increase in the gene number through gene and genome duplications followed by neo- and sub-functionalization has corresponded to the evolution of body organization in the land plants (Gramzow and Theissen, 2010; Harrison, 2017).

MIKC^{C}-type MADS-box genes have diverged remarkably and are involved in various developmental processes in angiosperms. On the other hand, their expression patterns were analysed in basal land plants and green algae. In gymnosperms, genomes of *Picea abies*, *Picea glauca*, and *Pinus taeda* were sequenced, and MIKC^{C}-type MADS-box genes were identified. They are expressed in roots, shoot apices, male cones, and female cones (Gramzow et al., 2014). The genes of *Gnetum gnemon* and *Gnetum parvifolium* are also expressed in male and female cones, and female cones and leaves, respectively (Becker et al., 2000; Shindo et al., 1999). In ferns, MIKC^{C}-type MADS-box genes are expressed in shoot apices, roots, leaves, male gametophytes, and sporangia of *Ceratopteris richardii* (Münster et al., 1997; Hasebe et al., 1998), and in

roots, leaves, prothallus, and sporangia of *Dryopteris fragrans* (Huang et al., 2014). In bryophytes, the MIKC^{C}-type MADS-box genes are expressed in protonemata, gametophore leaves, gametangia, and sporophytes of *Physcomitrella patens* (Hohe et al., 2002; Singer et al., 2007; Quodt et al., 2007). Each MIKC^{C}-type MADS-box gene in the green algae *Chara globularis* and *Closterium peracerosum–strigosum–littorale* complex is expressed in gametes and the timing of gametangium formation, respectively (Tanabe et al., 2005). Although expression patterns were analyzed, the functions of MIKC^{C}-type MADS-box genes are not clear in land plants outside of angiosperms and the green algae. In this study, the functions of MIKC^{C}-type MADS-box genes in *Physcomitrella patens* are examined to provide insights into the original role in the common ancestor of land plants and the functional evolution of MIKC^{C}-type MADS-box genes.

2. Introduction

Physcomitrella patens (Physcomitrella) is a member of basal land plants, and one of the model bryophytes. Six MIKC^{C}-type MADS-box genes, *PPM1*, *PPM2*, *PpMADS1* (Singer et al., 2007), *PPMC5*, *PPMC6* (Rensing et al., 2008), and *PpMADS-S* (Hohe et al., 2002) are identified in the Physcomitrella genome, and the first three genes form one clade, while the last three genes comprise another (Gramzow et al., 2012). Previous studies inferred the expression of a part of these genes with different strategies. A *uidA* reporter gene was inserted at the start codon of *PPM1*, *PPM2*, and *PpMADS1* to analyze their promoter activities by detecting the GUS signals (Singer et al., 2007). Promoter activity of *PPM1* and *PpMADS1* are detected in all cells in protonemata, gametophore leaves, antheridia, archegonia, and sporophytes, while that of *PPM2* was not detected in these cells. In another study (Quodt et al., 2007), *PPM2* expression is detected in a transgenic line in which a DNA fragment containing a *uidA* coding sequence is inserted to fuse *PPM2* at the 3' end of the exon 7. GUS signals are detected in whole antheridia and ventral parts of archegonia. When the *uidA* gene is replaced by the red fluorescent protein gene *DsRed*, the fluorescent signals are detected in protonemata, gametophore leaves, gametangia, and the sporophyte feet. Regarding *PpMADS-S* gene, transcripts are detected in both gametophores and sporophytes, and the amounts increase in gametophores under short-day and 15°C conditions (Hohe et al., 2002).

As the functional analysis, knockdown lines of *PPM1* using antisense RNA exhibit lower number of gametangia and sporophytes than the control line (Singer et al., 2007). Furthermore, young sporophytes become swollen and the sporophytes lack the protruding tip. In addition to these defects, the antisense lines show leaves curled spirally. These phenotypes are variable between different lines, and the deletion lines of

PPM1 gene were indistinguishable from the control line. Similarly, deletion lines of *PPM2* and *PpMADS1* were not distinguished from the control line (Singer et al., 2007). Overall, the functions of MIKC^C-type MADS-box genes in Physcomitrella remain unclear.

In this study, to elucidate the functions of the MIKC^C-type MADS-box genes in Physcomitrella and infer their evolution in land plants, the spatiotemporal localization patterns of all six Physcomitrella MIKC^C-type MADS-domain proteins were analysed and the morphology and development of the deletion mutant and over-expression lines were characterized. The MIKC^C-type MADS-domain proteins are expressed in both gametophyte and sporophyte in distinct but partially overlapping patterns. In addition, the MIKC^C-type MADS-box genes are necessary for proper fertilization in two ways: the regulation of the length of the gametophore internodes affecting the external water uptake, which enables the sperms to swim to the egg, and the regulation of motile flagella formation in the sperms. The former function appears to commonly exist in angiosperms, since internode length is determined by cell division and growth, which are also regulated by certain angiosperm MIKC^C-type MADS-box genes (Tapia-López et al., 2008; Borner et al., 2000; Michaels et al., 2003). The latter function was lost, consistent with the loss of sperm in the angiosperms.

3. Materials and Methods

3.1. Plant materials and culture conditions

Physcomitrella patens Bruch and Schimp. (Beike et al., 2014) Cove-NIBB (Nishiyama et al., 2000) line was cultured on BCDAT medium with 0.8% (w/v) agar at 25°C under continuous light conditions (Nishiyama et al., 2000) to generate protonema materials. Protonemata were transplanted into sterile peat pots (Jiffy-7; Jiffy Products International AS), half immersed in water, and cultured for a month at 25°C under continuous light to generate gametophores. To obtain gametangia and sporophytes, the peat pots containing gametophores were moved to 15°C under short-day (8 h light and 16 h dark) conditions (Sakakibara et al., 2008). To obtain gametophores with elongated internodes, the pots containing young gametophores were cultured in a red box (red-light conditions) or submerged in water (submergence conditions) for two to three weeks.

3.2. Transformation

The primer sequences, plasmids, and constructs used for the production of the GUS and Citrine fusions, deletion lines, and over-expression lines are shown in Table 1 and Figs. 1-7. Transformation was performed as described previously (Nishiyama et al., 2000). Stable GUS and Citrine fusion and deletion lines were screened using a DNA gel blot analysis to confirm single integrations. Over-expression lines were screened using PCR and quantitative RT-PCR analyses. All transgenic lines were examined to be haploid with flow cytometry as previously described (Ishikawa et al., 2011). The sextuple deletion mutant line #305 was made as follows: *PPM2* was deleted from the *ppm1* deletion mutant line #1, *PpMADS1* and *PPMC6* were simultaneously deleted from the

Table 1. Primers for construction and qRT-PCR.

Primers for the construction of GUS and Citrine fusion lines

Target gene		Sequence
PPM1	5'(F)	5'-TGCAATCGAACGGTATTTCTCGAGTTGTG-3'
	5'(R)	5'-ATTCTCACACTTGGTAAAATGTTTGCATGG-3'
	3'(F)	5'-AAAGTTACATTTCGATCGGTAAGCCTCTCC-3'
	3'(R)	5'-GGAAAAACTGCAAGCCTAAGTTAACG-3'
PPM2	5'(F)	5'-CTGAGTCTTCTCTTAAGCAATTTGACCAG-3'
	5'(R)	5'-ATTCTCACACTTGGTGATATGTTTGCATGG-3'
	3'(F)	5'-AACCATTCCACGTAGATTGGTAAGACACTC-3'
	3'(R)	5'-GTTTGCAGATGTCATTTGCTGCTGACACG-3'
PpMADS1	5'(F)	5'-GAGGGTATGGCACTCCTCTCACCTCTTG-3'
	5'(R)	5'-ACGCGTCGACTCGATCGACATGTAACTTATAAGTTCTC-3'
	3'(F)	5'-CACTTCGAACGACAGAAGGCTCTTTG-3'
	3'(R)	5'-GGTTCTTGTACATGGTAATGCAACATG-3'
PPMC5	5'(F)	5'-GCAGCGTTTCTCAAGCTTGTGTACTTCG-3'
	5'(R)	5'-TCTGACTTCTGTAGTGTGAATGTTCCCATCTC-3'
	3'(F)	5'-GACTCCATGCAATCTTTCCACCACAAGGAAAACAG-3'
	3'(R)	5'-CTAGAATAACGATGTAAGAGATGGAAGACTAAGAGTTG-3'
PPMC6	5'(F)	5'-CACTGATGCGCGTTACCTTTGACTTGC-3'
	5'(R)	5'-TCTGGCTTCGAAAGTGTGGATGTTCCC-3'
	3'(F)	5'-AGACTCCATGCAACCTTTCAACCACG-3'
	3'(R)	5'-GGCTGCCGAATGCAGTGATGTAAGG-3'
PpMADS-S	5'(F)	5'-CACCGTGAACTATGCCGCAAAGG-3'
	5'(R)	5'-CCTGACCCCTATACCGTTCCCATCTTATAG-3'
	3'(F)	5'-TAGAGTTCATGCAAACTTTCCATGAGCG-3'
	3'(R)	5'-CCAAGTGAATAACAGGGCTCCAGCATC-3'

Primers for the construction of the deletion lines

Target gene		Sequence
PPM1	5'(F)	5'-GTTATTGTTGGTTAATGTACAACTTCAC-3'
	5'(R)	5'-CACCCTTTCGCCGTGTCGACTCCGTGC-3'
	3'(F)	5'-AAAGTTACATTTCGATCGGTAAGCCTCTCC-3'
	3'(R)	5'-GGAAAAACTGCAAGCCTAAGTTAACG-3'
PPM2	5'(F)	5'-CAAGCCTACCACGAATGCCTAGTTG-3'
	5'(R)	5'-AACCCGACCCTTGGACCGCGACTC-3'
	3'(F)	5'-AACCATTCCACGTAGATTGGTAAGACACTC-3'

	3'(R)	5'-GTTTGCAGATGTCATTTGCTGCTGACACG-3'	
PpMADS1	5'(F)	5'-TGCTCTGGAGAGTGATAGCCCAATGC-3'	
	5'(R)	5'-CTCGACATCCCGAGCGACAAACACGTTGG-3'	
	3'(F)	5'-GCCACTTCGAACGACAGAAGGC-3'	
	3'(R)	5'-GAATTTTCATACACAAATAGATAATAATTTGAC-3'	
PPMC5	5'(F)	5'-GATTTCACTTGAATGTCCCACCAGTGC-3'	
	5'(R)	5'-AACCACCTCGCGCTCTTTGGGTG-3'	
	3'(F)	5'-GACTCCATGCAATCTTTCCACCACAAGGAAAACAG-3'	
	3'(R)	5'-CTAGAATAACGATGTAAGAGATGGAAGACTAAGAGTTG-3'	
PPMC6	5'(F)	5'-GGAGAGAGAGTAGAGGGATTTGAAGCAAGC-3'	
	5'(R)	5'-AACCACCTCACGCTCTTTCGGTGG-3'	
	3'(F)	5'-AGACTCCATGCAACCTTTCAACCACG-3'	
	3'(R)	5'-GGCTGCCGAATGCAGTGATGTAAGG-3'	(for with marker)
	3'(R)	5'-TGTCAGGGTACTGTCTATTCGAACAGGAGTG-3'	(for without marker)
PpMADS-S	5'(F)	5'-AGCGCTGAGCGCAAGGAATCTGG-3'	
	5'(R)	5'-GATGAGCTATCCAGCACTACACGACCG-3'	
	3'(F)	5'-TAGAGTTCATGCAAACTTTCCATGAGCG-3'	
	3'(R)	5'-CCAAGTGAATAACAGGGCTCCAGCATC-3'	

Primers for the construction of the overexpression lines

Target gene		Sequence
PPM1	(F)	5'-CACCATGATGACTGCGGCGTGTGGA-3'
	(R)	5'-TTATCGATCGACATGTAACT-3'
PPM2	(F)	5'-CACCATGACTGCGTCTGGACAATCCT-3'
	(R)	5'-CTAAATTCTCACACTTGGTGATATGTTTGCA-3'
PpMADS1	(F)	5'-CACCATGATGACTACAGCGTCTGGA-3'
	(R)	5'-TTATCGATCGACATGTAACT-3'
PPMC5	(F)	5'-CACCATGATGACAGCGTCTGGGCA-3'
	(R)	5'-CTACTTCTGACTTCTGTAGTGT-3'
PPMC6	(F)	5'-CACCATGACAGTGTCTGGACAGAACA-3'
	(R)	5'-CTATTTCTGGCTTCGAAAGTGTGGA-3'
PpMADS-S	(F)	5'-CACCATGACAGCCTCTGGACAGTACAGA-3'
	(R)	5'-CTATTCCTGACCCCTATACCGTT-3'

Primers for qRT-PCR

Target gene		Sequence
PPM1	(F)	5'-GGTGGCGCTGGTTATTTTCTC-3'
	(R)	5'-CCGAGCTGGCATACTCGAA-3'

PPM2	(F)	5'-TTCTGCACGGCGATTGTG-3'
	(R)	5'-GCACGCCACGCCTAGTG-3'
PpMADS1	(F)	5'-GATCCCCAGCACGGAAGA-3'
	(R)	5'-GCGGATGATCCCATTTCAAG-3'
PPMC5	(F)	5'-CGATGTGGCCCTCATCATTT-3'
	(R)	5'-GAGCTGGCGAATTCGAACA-3'
PPMC6	(F)	5'-GGCGAAAGGAGCACGACTT-3'
	(R)	5'-GCAAGCTTCTGACGCAATTCT-3'
PpMADS-S	(F)	5'-GGAGGTGCCGGTCGTGTA-3'
	(R)	5'-GGATCCACCTTTCCCACAAA-3'
TUA1	(F)	5'-CGTAGGAGGGACCAGTTTGG-3'
	(R)	5'-TGCATTCATCCCCGAGTCA-3'

(F): Forward primer

(R): Reverse primer

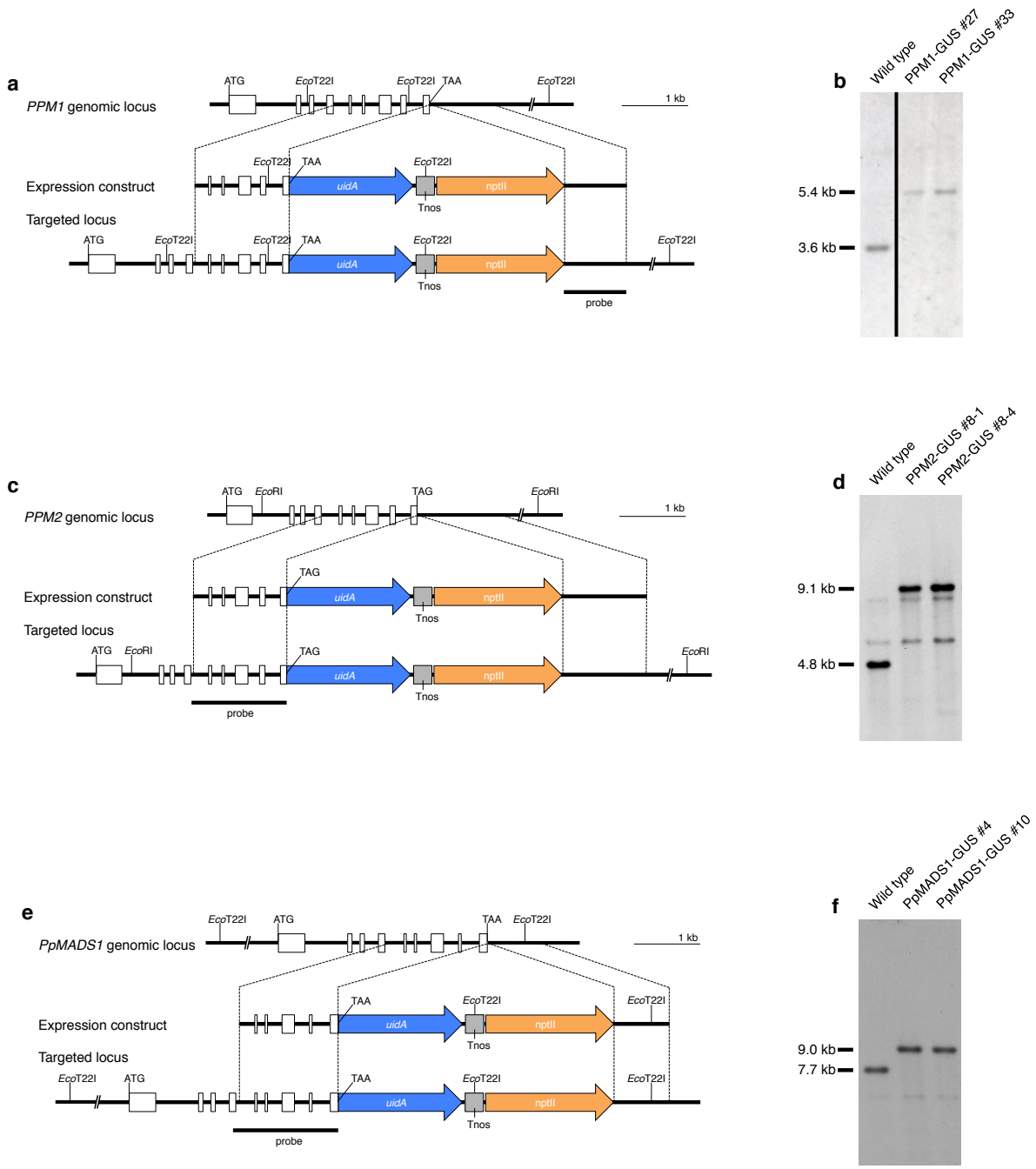

Figure 1 | Constructions of PPM1-, PPM2-, and PpMADS1-GUS fusion lines. a,c,e, Schematics of the *PPM1* (**a**), *PPM2* (**c**), and *PpMADS1* (**e**) loci and each targeting for insertion. White boxes represent the exons. Blue and orange arrows and grey boxes denote the *uidA* gene (GUS; Jefferson, 1987), the neomycin phosphotransferase II expression cassette (nptII; Nishiyama et al., 2000), and the terminator of the nopaline synthase gene (Tnos; Nishiyama et al., 2000) on the pTN85 plasmid (AB267707) for PPM1 and PPM2 and on the pGUSmutNPTII plasmid (LC279613) for PpMADS1, respectively. The probes used for DNA gel-blot analyses are indicated. **b,d,f**, DNA gel-blot analyses of targeted lines. Genomic DNAs of the wild type and the PPM1-GUS fusion lines #27 and #33 were digested with *Eco*T22I (**b**), the wild type and the PPM2-GUS fusion lines #8-1 and #8-4 were digested with *Eco*RI (**d**), and the wild type and the PpMADS1-GUS fusion lines #4 and #10 were digested with *Eco*T22I (**f**), respectively.

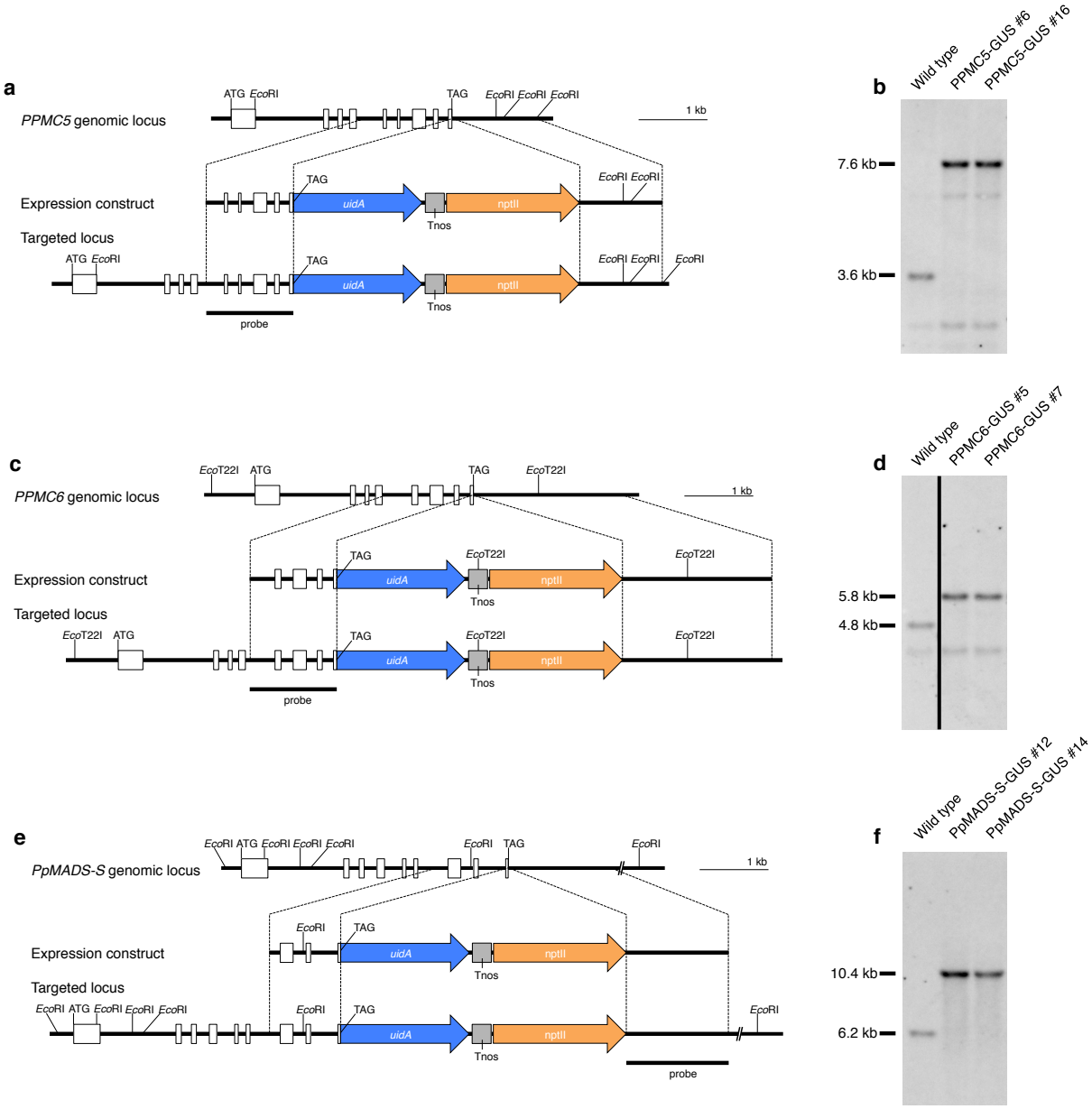

Figure 2 | Constructions of PPMC5-, PPMC6, and PpMADS-S-GUS fusion lines. a,c,e, Schematics of the *PPMC5* (**a**), *PPMC6* (**c**), and *PpMADS-S* (**e**) locus and each targeting for insertion. White boxes represent the exons. Blue and orange arrows and grey boxes denote the *uidA* gene (GUS; Jefferson, 1987), the neomycin phosphotransferase II expression cassette (nptII; Nishiyama et al., 2000), and the terminator of the nopaline synthase gene (Tnos; Nishiyama et al., 2000) on the pTN85 plasmid (AB267707), respectively. The probes used for DNA gel-blot analyses are indicated. **b,d,f**, DNA gel-blot analyses of targeted lines. Genomic DNAs of the wild type and the PPMC5-GUS fusion lines #6 and #16 were digested with *Eco*RI (**b**), the wild type and the PPMC6-GUS fusion lines #5 and #7 were digested with *Eco*T22I (**d**), the wild type and the PpMADS-S-GUS fusion lines #12 and #14 were digested with *Eco*RI (**f**), respectively.

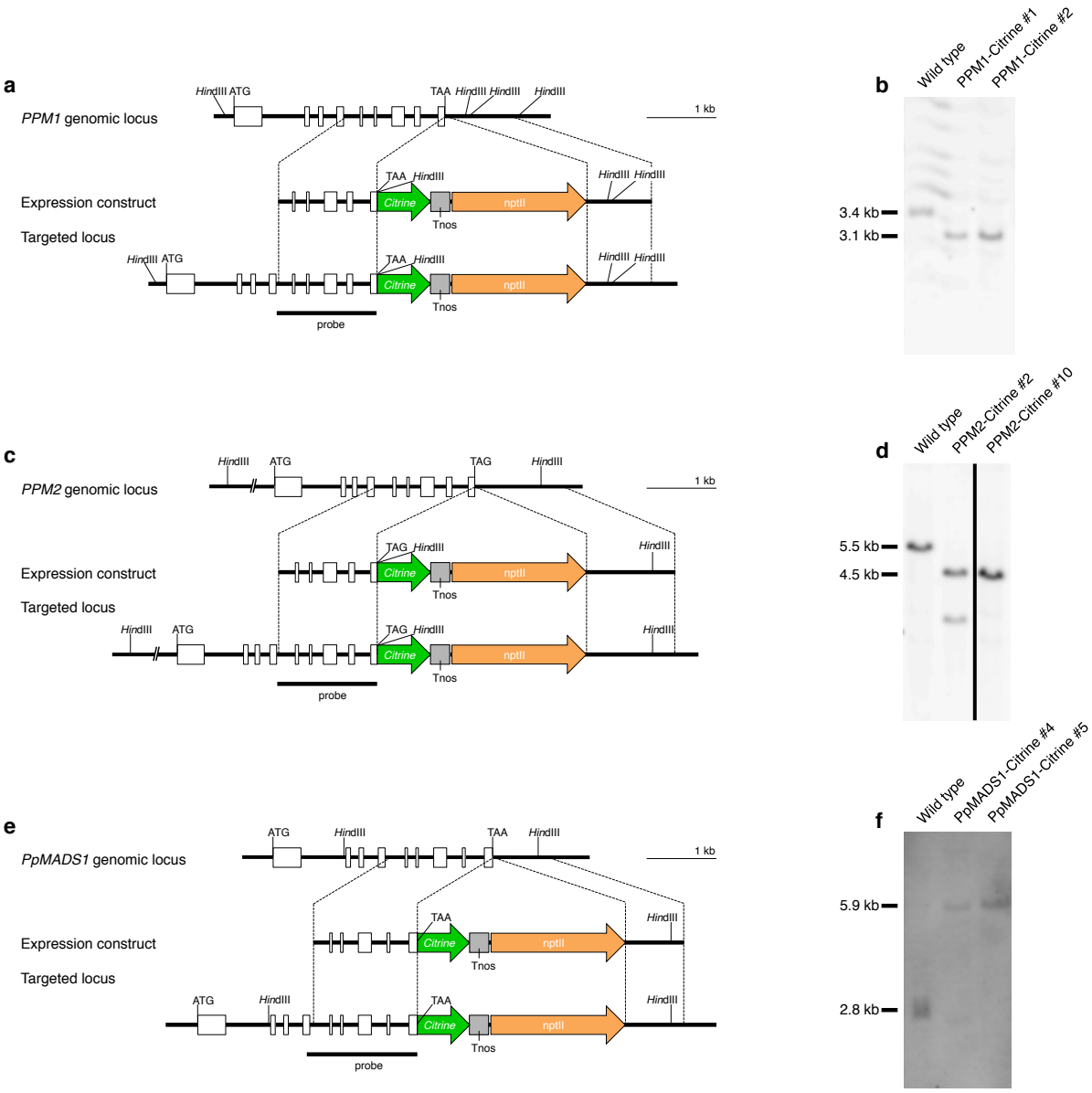

Figure 3 | Constructions of PPM1-, PPM2-, and PpMADS1-Citrine fusion lines. a,c,e, Schematics of the *PPM1* (**a**), *PPM2* (**c**), and *PpMADS1* (**e**) loci and each targeting for insertion. White boxes represent the exons. Green and orange arrows and grey boxes denote the yellow fluorescent protein gene *Citrine* (Griesbeck et al., 2001), the neomycin phosphotransferase II expression cassette (nptII; Nishiyama et al., 2000), and the terminator of nopaline synthase gene (Tnos; Nishiyama et al., 2000) on the pCTRN-NPTII-2 plasmid (AB697058), respectively. The probes used for DNA gel-blot analyses. **b,d,f**, DNA gel-blot analyses of targeted lines. Genomic DNAs of the wild type and the PPM1-Citrine fusion lines #1 and #2 were digested with *Hin*dIII (**b**), the wild type and the PPM2-Citrine fusion lines #2 and #10 were digested with *Hin*dIII (**d**), and the wild type and the PpMADS1-Citrine fusion lines #4 and #5 were digested with *Hin*dIII (**f**), respectively.

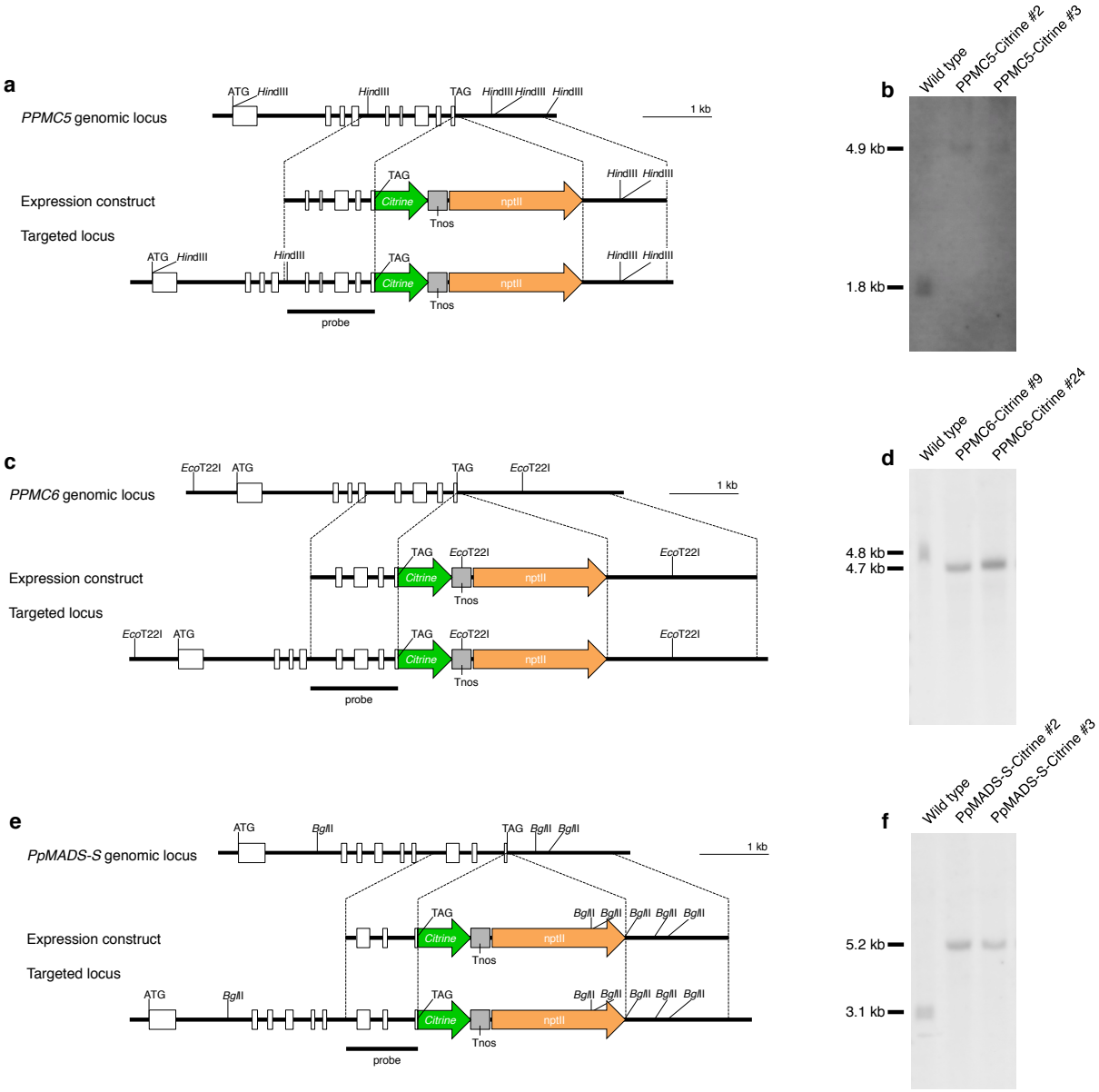

Figure 4 | Constructions of PPMC5-, PPMC6-, and PpMADS-S-Citrine fusion lines. a,c,e, Schematics of the *PPMC5* (**a**), *PPMC6* (**c**), and *PpMADS-S* (**e**) loci and each targeting for insertion. White boxes represent the exons. Green and orange arrows and grey boxes denote the yellow fluorescent protein gene *Citrine* (Griesbeck et al., 2001), the neomycin phosphotransferase II expression cassette (nptII; Nishiyama et al., 2000), and the terminator of nopaline synthase gene (Tnos; Nishiyama et al., 2000) on the pCTRN-NPTII-2 plasmid (AB697058), respectively. The probe used for DNA gel-blot analyses are indicated. **b,d,f**, DNA gel-blot analyses of targeted lines. Genomic DNAs of the wild type and the PPMC5-Citrine fusion lines #2 and #3 were digested with *Hin*dIII (**b**), of the wild type and the PPMC6-Citrine fusion lines #9 and #24 were digested with *Eco*T22I (**d**), and the wild type and the PpMADS-S-Citrine fusion lines #2 and #3 were digested with *Bgl*II (**f**), respectively.

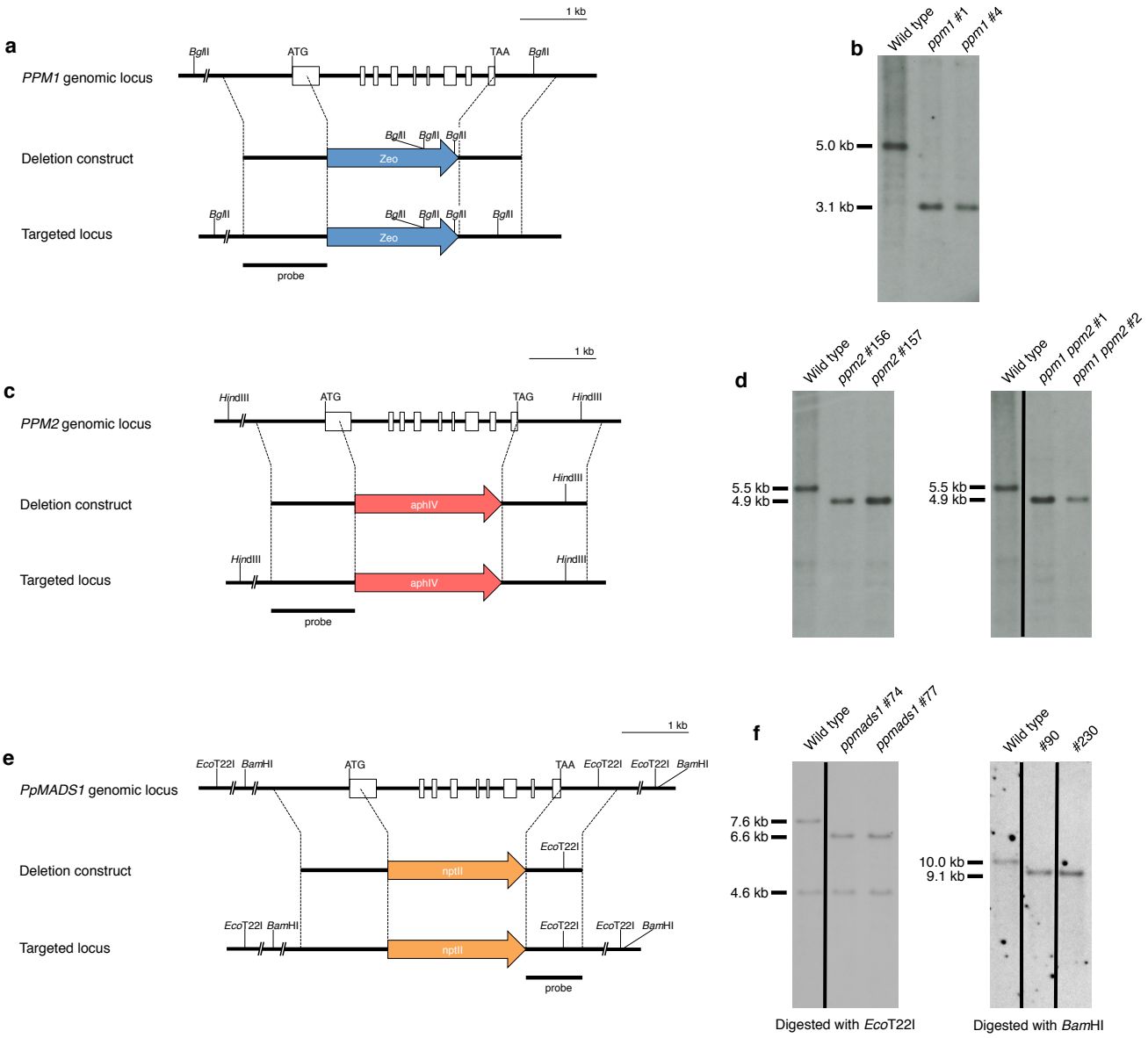

Figure 5 | Deletion constructs of *PPM1*, *PPM2*, and *PpMADS1* genes. a,c,e, Schematic of the *PPM1* (**a**), *PPM2* (**c**), and *PpMADS1* (**e**) loci and each targeting for insertion. White boxes represent the exons. Blue (**a**), red (**c**), and orange (**e**) arrows denote the Zeocin resistance expression cassette (Zeo; Sakakibara et al., 2008) on the p35S-Zeo plasmid (EF451822), the aminoglycoside phosphotransferase IV expression cassette (aph IV; Hiwatashi et al., 2008) on the pHTS14 plasmid (Tanahashi et al., 2005), and the neomycin phosphotransferasee II expression cassette (nptII; Nishiyama et al., 2000) on the pTN82 plasmid (AB720111), respectively. The probes used for DNA gel-blot analyses are indicated. **b,d,f**, DNA gel-blot analyses of targeted lines. Genomic DNAs of the wild type, the *ppm1* mutant line #1, and the *ppm1* mutant line #4 were digested with *Bgl*II (**b**), the wild type, the *ppm2* mutant line #156, the *ppm2* mutant line #157, the *ppm1 ppm2* mutant line #1, and the *ppm1 ppm2* mutant line #2 were digested with *Hin*dIII (**d**), and the wild type, the *ppmads1* mutant line #74 and the *ppmads1* mutant line #77 were digested with *Eco*T22I (**f**, left), while DNAs from the wild type, *ppm1 ppm2 ppmads1 ppmc6* mutant line #90, and *ppm1 ppm2 ppmads1 ppmads-s* mutant line #230 were digested with *Bam*HI (**f**, right).

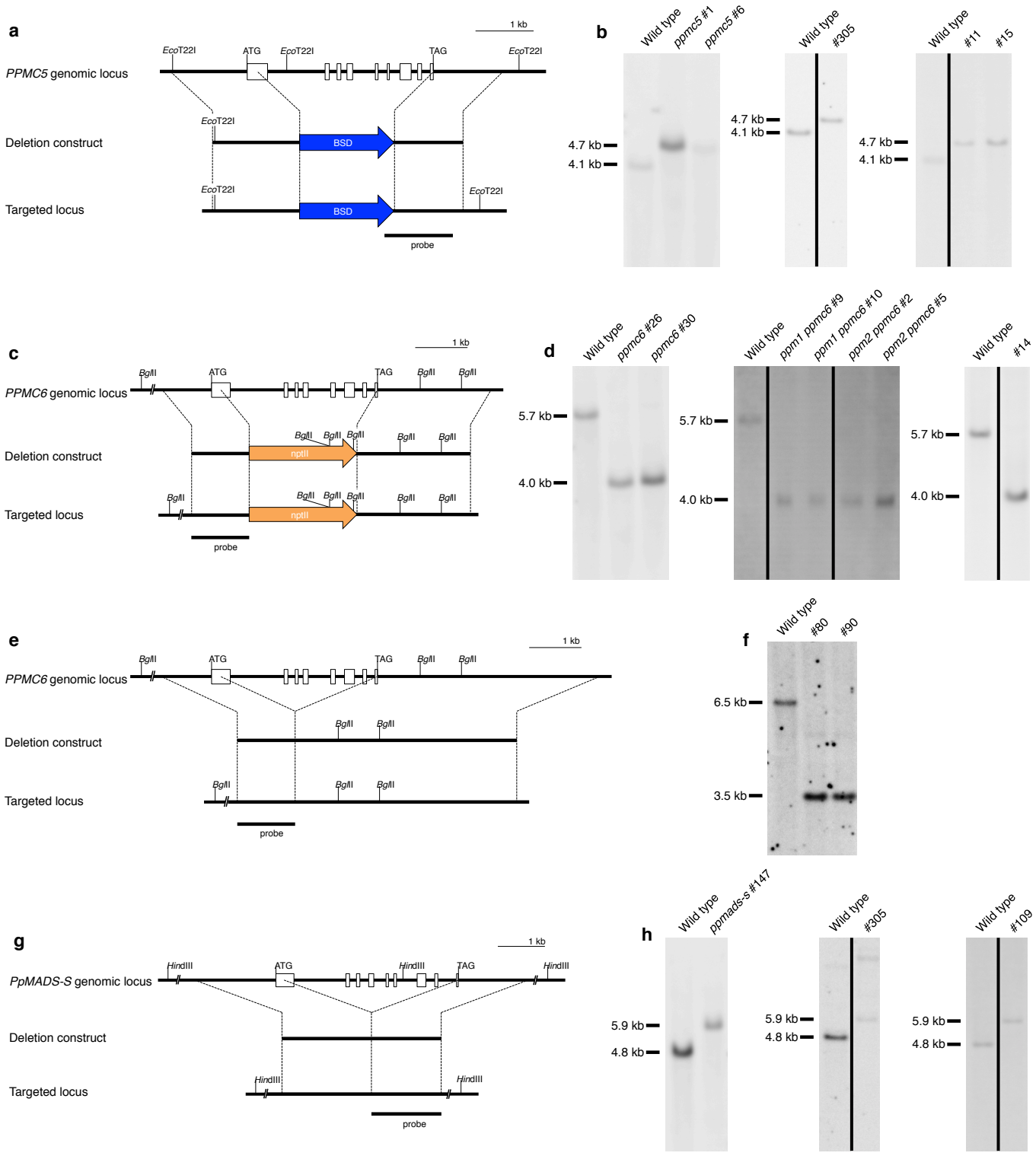

Figure 6 | Deletion constructs of *PPMC5*, *PPMC6*, and *PpMADS-S* genes. a,c,e,g, Schematics of the *PPMC5* (**a**), *PPMC6* (**c,e**), *PpMADS-S* (**g**) loci and each targeting for insertion. White boxes represent the exons. Blue and orange arrows denote the Blasticidin resistance expression cassette (BSD; Ishikawa et al., 2011) on the p35S-BSD2 plasmid (LC279014) and the neomycin phosphotransferasee II expression cassette (nptII; Nishiyama et al., 2000) on the pTN182 plasmid (AB267706), respectively. The probes used for , DNA gel-blot analyses are indicated. **b,d,f,h**, DNA gel-blot analyses of targeted lines. Genomic DNAs of the wild type, the *ppmc5* mutant line #1, the *ppmc5* mutant line #6, the *ppm1 ppm2 ppmads1 ppmc5 ppmc6 ppmads-s* mutant line #305, the *ppm1 ppm2 ppmads1 ppmc5 ppmc6* mutant line #11, and the *ppm1 ppm2 ppmads1 ppmc5 ppmc6* mutant line #15 were digested with *Eco*T22I (**b**), the wild type, the *ppmc6* mutant line #26, the *ppmc6* mutant line #30, and the *ppm1 ppm2 ppmc6* triple deletion mutant line #14 were digested with *Bgl*II (**d**), the wild type, the *ppm1 ppm2 ppmc6* mutant line #80, and the *ppm1 ppm2 ppmads1 ppmc6* mutant line #90 were digested with *Bgl*II (**f**), and the wild type, the *ppmads-s* mutant line #147, the *ppm1 ppm2 ppmads1 ppmc5 ppmc6 ppmads-s* mutant line #305, and the *ppm1 ppm2 ppmads1 ppmc5 ppmc6 ppmads-s* mutant line #109 were digested with *Hin*dIII (**h**).

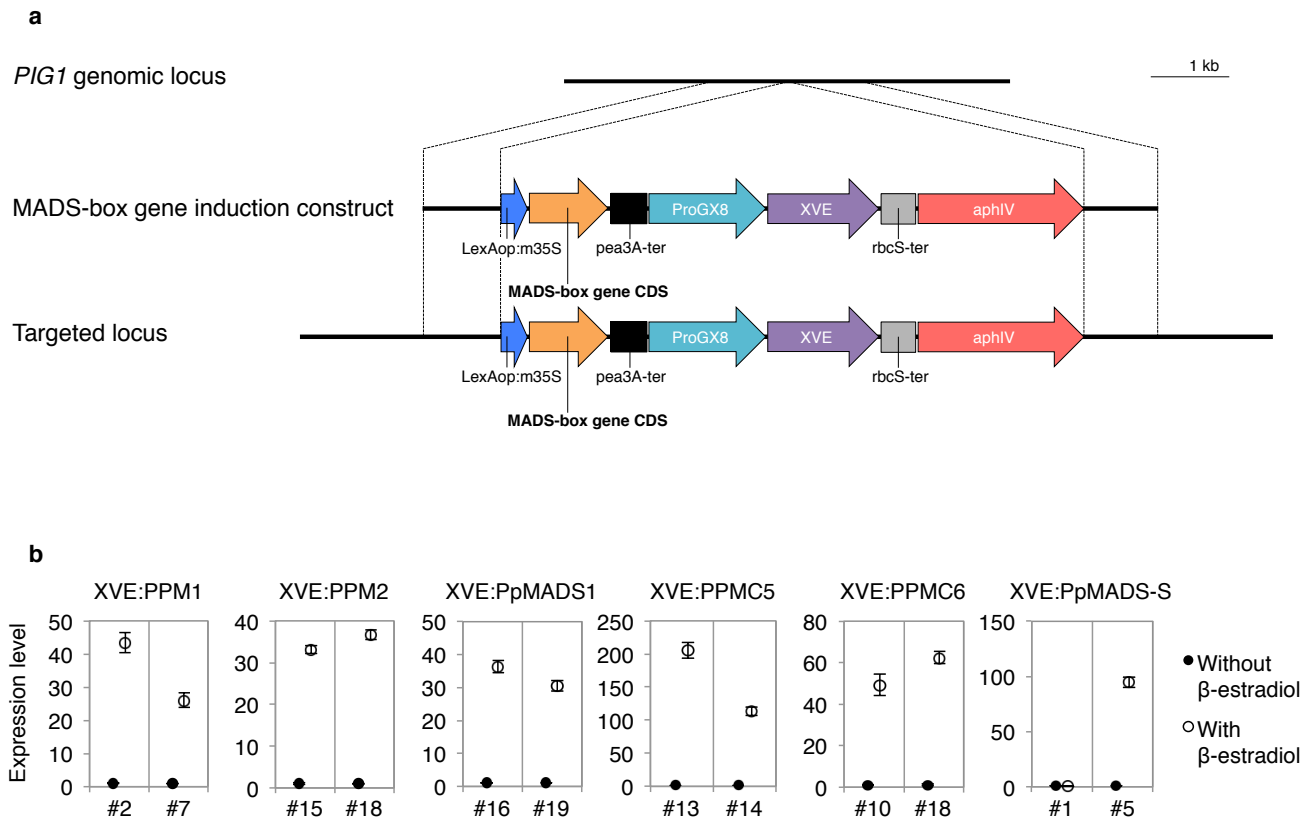

Figure 7 | Construction of over-expression lines of each of the six MIKC^{C}-type MADS-box genes using the β-estradiol induction system. a, A schematic of six MIKC^{C}-type MADS-box gene induction constructs targeted to the *PIG1* neutral locus (Okano et al., 2009). Blue, orange, light blue, purple, and red arrows denote the LexA operator and minimal 35S promoter (LexAop;m35S; Zuo et al., 2000), a coding nucleotide sequence (CDS) of each MADS-box gene, the GX8 promoter (ProGX8; Kubo et al., 2013), a DNA fragment encoding a XVE fusion protein derived from pER8 (Zuo et al., 2000), and the aminoglycoside phosphotransferase IV expression cassette (aph IV; Hiwatashi et al., 2008), respectively. Black and grey boxes indicate the pea rbcS3A terminator (pea3A-ter; Fluhr et al., 1986) and the rbcS terminator (rbcS-ter; Fluhr et al., 1986), respectively. The CDS fragments were cloned into the pPGX8 plasmid (AB537482). **b**, Expression levels of MIKC^{C}-type MADS-box genes with β-estradiol are indicated as a multiple of those without β-estradiol.

ppm1 ppm2 mutant line #1, and *PPMC5* and *PpMADS-S* were simultaneously deleted from *ppm1 ppm2 ppmads1 ppmc6* #90. The sextuple deletion mutant line #109 was made as follows: *PPMC5* was deleted from *ppm1 ppm2 ppmads1 ppmc6* #90, then *PpMADS-S* was deleted from *ppm1 ppm2 ppmads1 ppmc5 ppmc6* #11. The triple deletion mutant lines #14 and #80 were made by deleting *PPMC6* from *ppm1 ppm2* mutant line #1.

3.3. DNA gel blot analysis

Genomic DNA was digested with restriction enzymes, run on 0.7% (w/v) SeaKem GTG agarose (Lonza), and transferred to a Hybond N+ nylon membrane (GE Healthcare). Probe labelling, hybridization, and detection were performed using the AlkPhos direct labelling and detection system with CDP-Star (GE Healthcare).

3.4. Microscopy analysis

Images and videos were taken using fluorescence microscopes SZX16 and BX51 (Olympus) equipped with colour cameras DP71 (Olympus) and DS-Fi1c (Nikon), respectively. Citrine fluorescent images were taken using a confocal laser microscope (SP8; Leica Microsystems), with a detecting fluorescence emission of 515–550 nm under excitation at 514 nm. For archegonia with sperm, mature archegonia (stage 9; Landberg et al., 2013) were fixed with 8% glutaraldehyde, stained using DAPI (1 μg ml^{-1}), and observed using a confocal laser microscope (A1R; Nikon) with a detecting fluorescence emission of 423–478 nm under excitation at 405 nm. For sperm movement, images and videos were taken using a dark-field microscope (BX60; Olympus) equipped with a CCD camera (ORCA-R2; Hamamatsu Photonics), and the videos for

five seconds were used for quantification of movement. Sperms were extracted by pressing the antheridia between a glass slide and a cover slip, and only isolated and mature sperms with spiral shape were observed.

3.5. Protein expression using the oestrogen inducing system

Gametophores were cultured on sterile peat pots for two weeks before being treated with 2.0 μM β-estradiol (Wako) dissolved in water. The gametophores were cultured for two weeks under continuous light conditions at 25°C.

3.6. Quantitative RT-PCR analysis

RNA was extracted and purified using an RNeasy Plant Mini Kit (Qiagen) and DNase I (Qiagen). First-strand cDNA was synthesized using ReverTraAce qPCR RT Master Mix (Toyobo), and qRT-PCR was performed using an ABI 7500 RealTimePCR System (Thermo Fisher Scientific) with a QuantiTect SYBR Green PCR Kit (Qiagen). Results were analysed using 7500 software version 2.3 (Thermo Fisher Scientific). The quantification of each sample was performed in triplicate.

3.7. Transcriptome analyses

For the gametophores, RNA was extracted using PureLink Plant RNA Reagent (Thermo Fisher Scientific) and purified with a RNeasy Plant Mini Kit (Qiagen) and DNase I (Qiagen). RNA-seq libraries were prepared using a TruSeq Stranded mRNA Library Prep Kit (Illumina). For the antheridia transcriptome, frozen antheridia from three shoot apices were ground in 50 μl RLT buffer (Qiagen) using 5 mm and 0.5 mm zirconia beads, then 10 μl supernatant was used for a single-cell RNA-seq method (Quartz-Seq;

Sasagawa et al., 2013). Sequencing was conducted using a HiSeq 2500 (Illumina) and 50 bp reads were obtained. For the reads of both the gametophore and antheridia transcriptomes, adapter and low-quality sequences were removed from the reads using cutadapt (version 1.9.1). The reads were mapped to transcript sequences of *Physcomitrella patens* version 3.0 (Ppatens_251_v3.0.transcript.fa) obtained via Phytozome (DOE-JGI; https://phytozome.jgi.doe.gov/) and calculated using RSEM (version 1.2.25) with Bowtie. DEGs between the wild type and the mutant lines with a q-value < 0.05 were extracted with an R package, TCC (Sun et al., 2013) and then DEGs with a fold change > 1.5 were selected. RNA-seq analyses for the gametophores were performed in biological triplicate and Quartz-Seq analyses for the antheridia were in biological quadruplicate. Published microarray data for each Arabidopsis MIKC^{C}-type MADS-box gene (*AP1*; Kaufmann et al., 2010, *AP3*; Wuest et al., 2012, *PI*; Wuest et al., 2012, *AG*; Maoiléidigh et al., 2013, *SOC1*; Seo et al., 2009; Tao et al., 2012, and *SVP*; Gregis et al., 2013) were compared with the Physcomitrella DEGs present between the wild type and the deletion mutant lines. Flagellum-related genes were identified from the antheridia DEGs by comparison with the 360 and 292 high and moderate confidence genes, respectively, identified in the flagella of the green alga *Chlamydomonas reinhardtii* (Pazour et al., 2005).

3.8. Observation by TEM

To visualize the cuticle, gametophore leaves and stems were fixed overnight at 4°C in a 0.05 M PIPES buffer (pH 7.0) containing 1.5% glutaraldehyde and 1.5% formaldehyde. Samples were washed three times with 0.05 M PIPES buffer for 20 min each, and osmium fixation was performed by placing the samples in 2% OsO_4 in 0.05 M PIPES

buffer (pH 7.0) for 2 h in the dark at 4°C, followed by washing them three times with distilled water for 30 min each. Dehydration was performed using a graded EtOH series (30, 50, 70, 90, and 100%) for 30 min at each stage, with two final rinses of 100% EtOH for 15 min each (Budke et al., 2011). The fixed tissues were embedded in LR White resin (London Resin Company Ltd.) and polymerized at 60°C for 1 d. Sectioning was performed using an Ultracut UCT Ultramicrotome (Leica Microsystems) at 70 nm. The sections were stained with uranyl acetate and lead citrate and observed using a JEM1010 (JEOL) TEM at 80 kV. For TEM observations of flagella, we used the previously described method (Ohara et al., 1998) with modifications. Flagella were fixed in 10% tannic acid and 2% glutaraldehyde for 1 h on ice. Samples were washed three times with 0.05 M Na-phosphate buffer (pH 7.0) for 15 min each, and were fixed in 2% OsO_4 in 0.05 M Na-phosphate buffer (pH 7.0) for 1 h on ice. The samples were then washed three times with distilled water for 15 min each. Dehydration was performed using a graded EtOH series (30, 50, 70, 90, and 100%) for 30 min at each stage, with two final rinses of 100% EtOH for 15 min each. After this step, tissues were embedded in Epon resin (TAAB Laboratories Equipment) and polymerized at 60°C for 1 d. Sectioning was performed using an Ultracut UCT Ultramicrotome (Leica Microsystems) at 50 nm. The sections were stained with uranyl acetate and lead citrate and observed using a JEM1010 (JEOL Ltd.) TEM at 80 kV.

3.9. Extracellular lipid identification and quantification

The extracellular lipids of *Physcomitrella patens* were identified and quantified using previously described methods with a minor modification (Greer et al., 2007; Kondo et al., 2016). The total extracellular lipids were extracted by immersing the gametophores

into chloroform for 30 s at room temperature, and n-tetracosane (C_{24} alkane) and behenyl oleate (C_{40} wax ester) were added as internal standards. The solution was dried under a stream of N_2 gas, and the residues were incubated with 50 µl BSTFA-TMCS and 50 µl pyridine for 1 h at 80°C. The BSTFA and pyridine were then removed under a stream of N_2 gas. The samples were re-dissolved in chloroform and analysed using a gas chromatography-mass spectrometer (GC-MS; GCMSTQ-8030; Shimadzu) equipped with a Rxi-5HT column (length, 15 m; internal diameter 0.25 mm; film thickness 0.1 µm; Restek) for the identification of the wax components. The samples were also analysed using gas chromatography-flame ionization detector (GC-FID; GC2014; Shimadzu) equipped with a Rxi-5HT column (length, 15 m; internal diameter 0.25 mm; film thickness 0.1 µm; Restek) for the quantification of the wax components. For the GC-MS and GC-FID, the carrier gas was helium, the injection port temperature was 320°C, and the column temperature was programmed as follows: 50°C for 5 min, increasing to 200°C at a rate of 40°C per min and held for 2 min, then raising to 380°C at a rate of 3°C per min and held for 10 min. The extracellular lipids were quantified by comparing the FID peak areas against the internal standards.

3.10. Reactivation experiment for sperm

Sperms were extracted from the antheridia by pressing them between a glass slide and a cover slip with a 0.3-mm spacer. After waiting for the sperm bodies to adhere to the glass slide, they were treated with 0.1% NP-40 substitute (Wako) in 30 mM HEPES (pH 7.4), 5 mM $MgSO_4$, 1 mM DTT, 1 mM EGTA, and 50 mM K-acetate to induce de-membranation. A reactivation solution (30 mM HEPES [pH 7.4], 5 mM $MgSO_4$, 1 mM DTT, 1 mM EGTA, 50 mM K-acetate, 1% polyethylene glycol [6,000 mol wt], and

1 mM ATP) was added to the de-membraned flagella using a modified method (Kamiya and Witman, 1984), and the sperms with reactivated flagella were counted.

4. Results

4.1. Localization of MIKC^{C}-type MADS-domain proteins fused with reporter proteins

Six MIKC^{C}-type MADS-box genes, *PPM1*, *PPM2*, *PpMADS1*, *PPMC5*, *PPMC6*, and *PpMADS-S* were previously identified in the genome of Physcomitrella and their proteins share from 54.9% to 87.8% identity in amino acid sequences (Fig. 8). The first three genes form one clade, while the last three genes comprise another (Fig. 9; Gramzow et al., 2012). To analyse the localisations of the corresponding proteins, a DNA fragment containing *uidA* or a modified yellow fluorescent protein gene, *Citrine*, were inserted just before the stop codon of each MIKC^{C}-type MADS-box gene by homologous recombination (Figs. 1-4), and GUS or Citrine fusion lines were generated. GUS and Citrine signals were detected in similar tissues and cells for each gene between GUS and Citrine fusion lines (Figs. 10 and 11), although Citrine signals and autofluorescence in the antheridia were indistinguishable (Fig. 11e). The localization of all six proteins was analysed over the course of the lifecycle (Fig. 12). Each spore cell divides to form a chloronema apical stem cell, which continuously divides to produce a filament of chloronema cells. After several divisions, the chloronema apical stem cells become caulonema apical stem cells, producing caulonema cells with a different chloroplast shape and cell septum angle from those of chloronema cells. GUS and Citrine signals of both the PPMC5 and PPMC6 fusion proteins were detected in the chloronema and caulonema cells (Figs. 10a,b and 11a,b). PPM1- and PPM2-Citrine signals were also detected in chloronemata and caulonemata, but were weaker than those of PPMC5 and PPMC6 (Fig. 11a,b). Some caulonema cells produce gametophore stem cells, each of which forms a leafy shoot known as the gametophore. Different

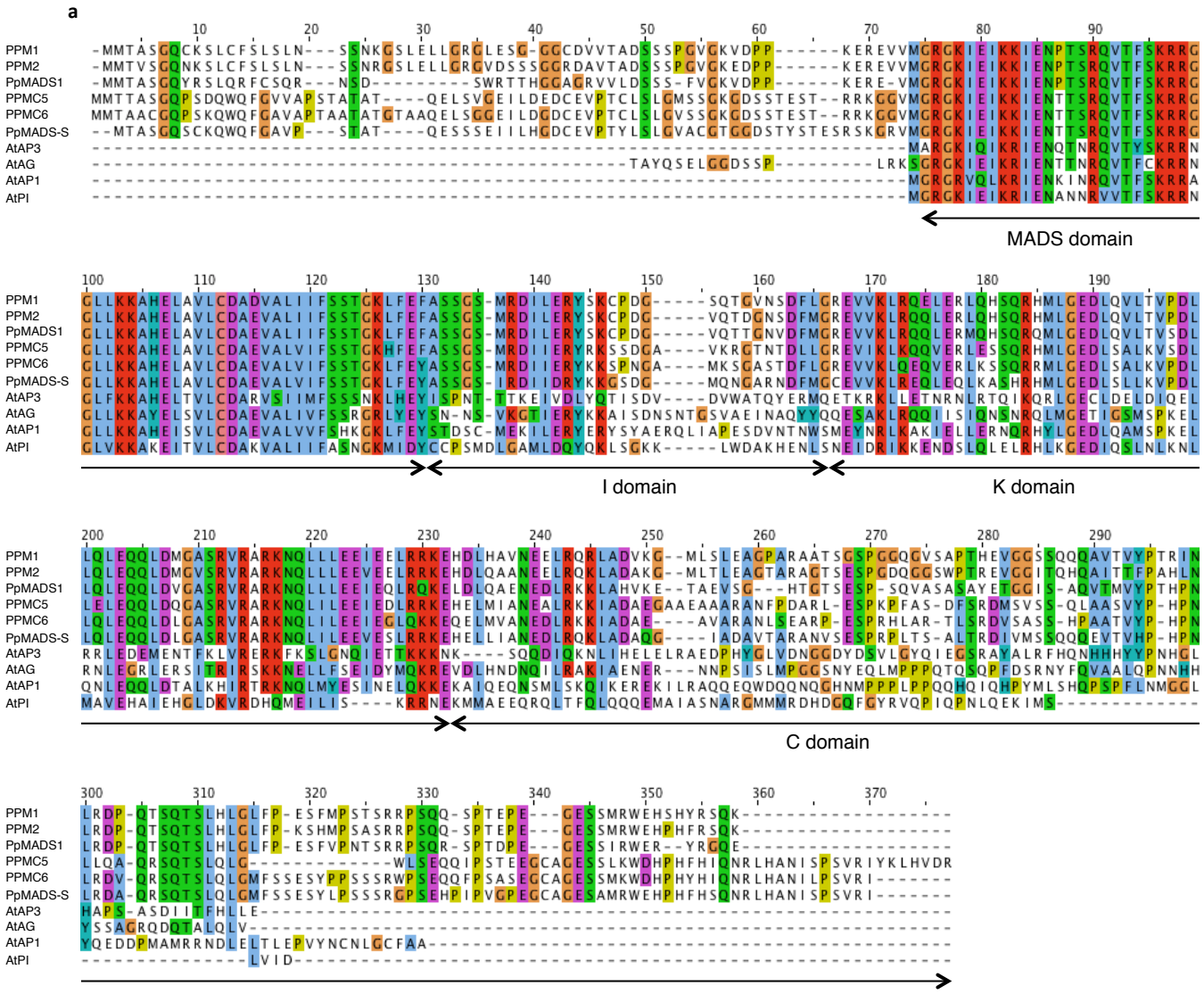

b

		Target					
	Identity (%)	PPM1	PPM2	PpMADS1	PPMC5	PPMC6	PpMADS-S
Query	PPM1		72.3	76.8	59.0	63.9	63.4
	PPM2	72.3		67.5	59.9	64.1	64.9
	PpMADS1	76.5	67.5		54.9	58.6	62.1
	PPMC5	57.8	66.1	58.1		87.8	77.8
	PPMC6	59.5	67.5	58.6	87.8		77.5
	PpMADS-S	64.2	63.8	62.1	72.4	71.6	

Figure 8 | Comparisons of amino acid sequences in six MIKC^{C}-type MADS-box proteins. a, Alignment of six proteins using Jalview 2.10.1 (Waterhouse et al., 2009) with ClustalWS (Larkin et al., 2007). Domain structure was designated according to previous studies (Riechmann et al., 1996). **b**, Percentages of identical amino acid residues between six MIKC^{C}-type MADS-box proteins.

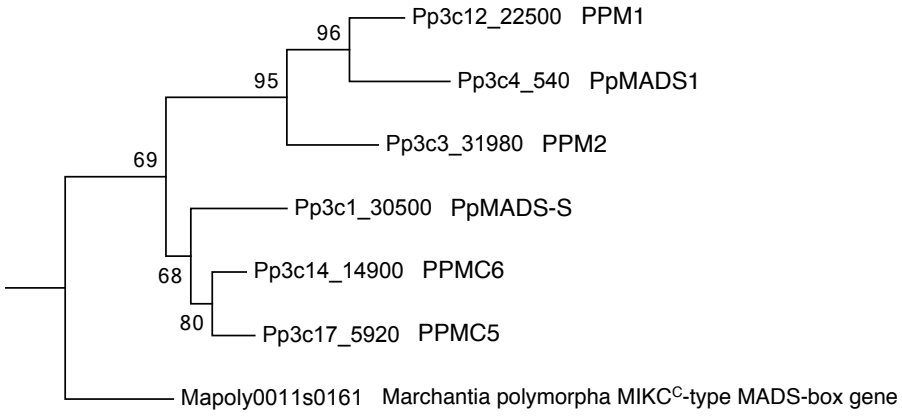

Figure 9 | Phylogenetic tree of six MIKC^{C}-type MADS-box proteins in Physcomitrella. Amino acid sequences were obtained via Phytozome (DOE-JGI, https://phytozome.jgi.doe.gov/). Alignment of amino acid sequences and construction of phylogenetic tree were performed using MEGA 6.06 with ClustalWS (Larkin et al., 2007) and method of maximum likelihood, respectively.

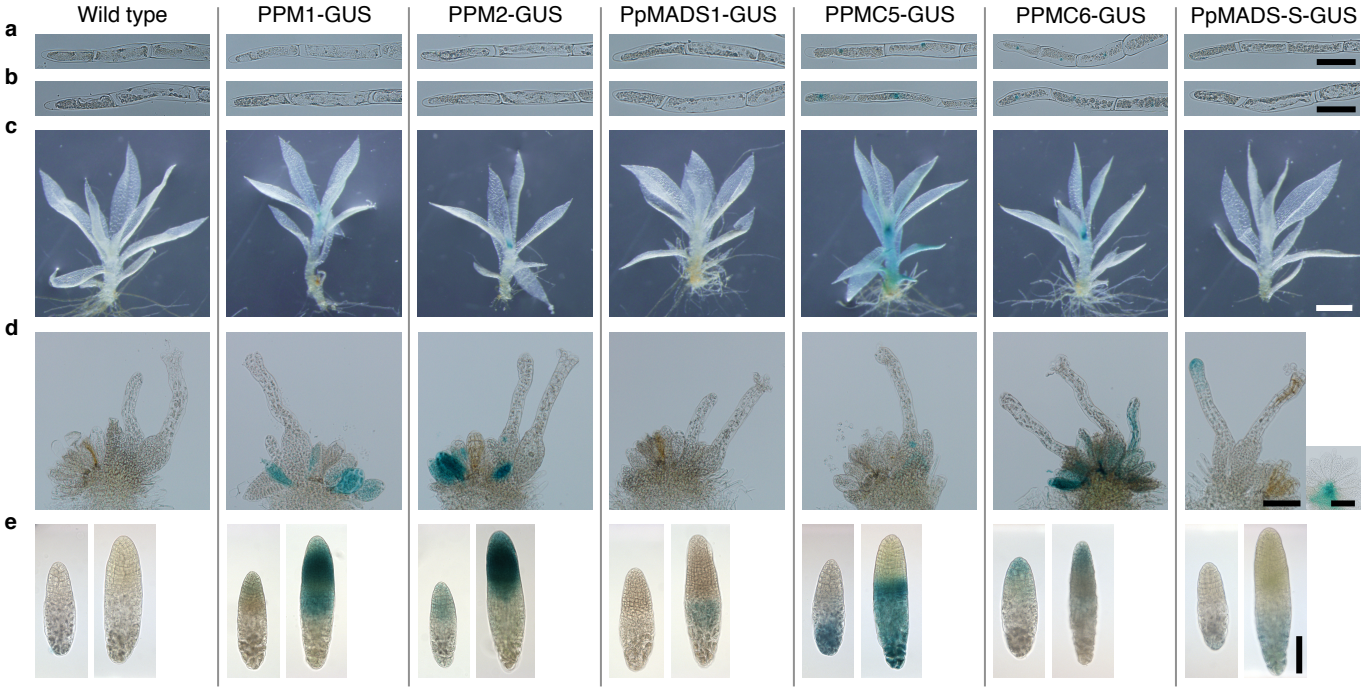

Figure 10 | Localization of MIKC^{C}-type MADS domain proteins fused with GUS reporter proteins. a-e, PPM1, PPM2, PpMADS1, PPMC5, PPMC6, and PpMADS-S were fused with GUS proteins. The localizations were investigated in the chloronema filaments (**a**); caulonema filaments (**b**); gametophores (**c**); antheridia and archegonia formed at the tip of the gametophores (**d**); and the developing sporophytes (**e**). Scale bars, 50 µm in **a**,**b**,**e**; 0.5 mm in **c**; 100 µm in **d**.

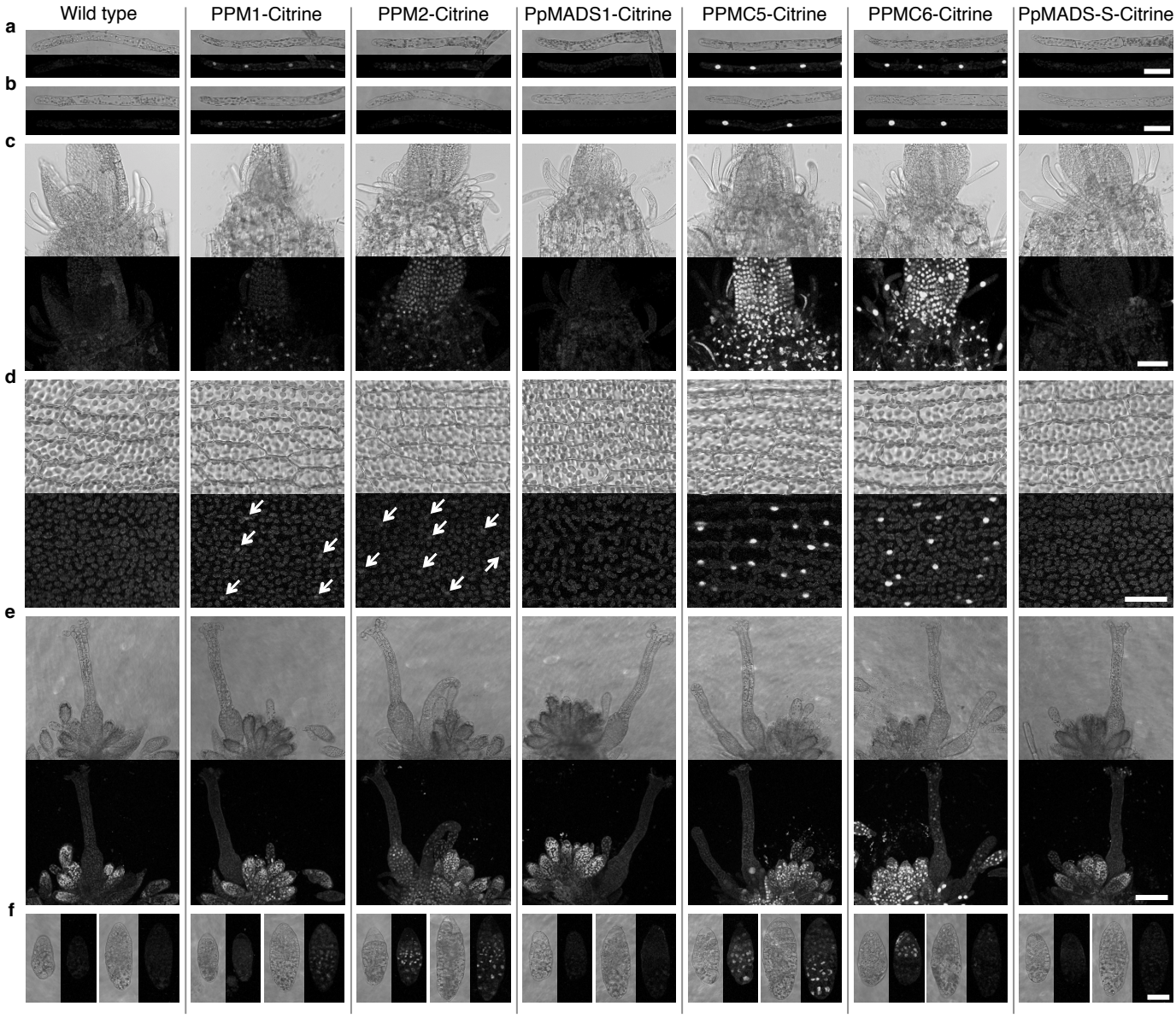

Figure 11 | Localization of MIKC^{C}-type MADS domain proteins fused with Citrine reporter protein. a-f, The localizations were investigated in the chloronema filaments (**a**); caulonema filaments (**b**); gametophore apices from which a part of the surrounding leaves were removed (**c**); mature gametophore leaf cells (**d**); antheridia and archegonia (**e**); and the developing sporophytes (**f**). Upper and lower panels indicate differential interference contrast images and fluorescent images, respectively. Maximum intensity projections of all slices of the z-stack are shown. White arrows in **d** indicate fluorescence signals of nuclei. Scale bars, 50 μm in **a**,**b**,**c**,**d**,**f**; 100 μm in **e**.

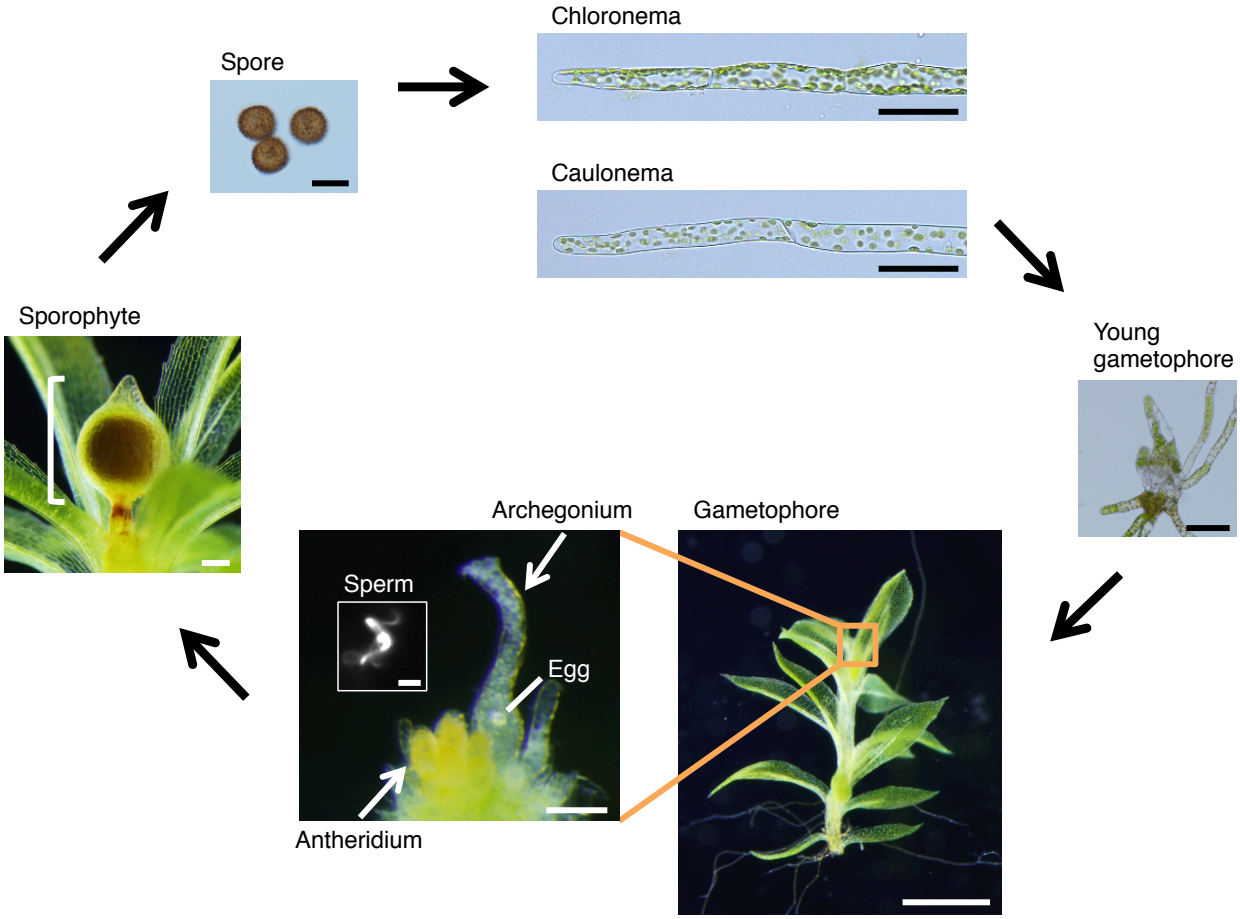

Figure 12 | Lifecycle of Physcomitrella. Scale bars, 50 µm in chloronema, caulonema, and young gametophore; 1 mm in gametophore; 50 µm in archegonium and antheridium; 5 µm in sperm; 200 µm in sporophyte; 30 µm in spore.

intensities of GUS signals for four proteins (PPM1, PPM2, PPMC5, and PPMC6) were detected at the tips of the gametophores (Fig. 10c), and GUS signals for PPMC5 were present throughout the gametophores (Fig. 10c). Citrine signals of the four proteins indicated their localization in young gametophore leaf cells and cells of stems at the base of young gametophore leaves (Fig. 11c), as well as in mature gametophore leaf cells (Fig. 11d). The antheridium and archegonium, which produce the sperm and the egg cell respectively, are formed at the tip of the gametophores when moss is cultivated under gametangium-inductive conditions (Sakakibara et al., 2008). GUS signals for PPM1, PPM2, and PPMC6 were detected in the antheridia (Fig. 10d), and GUS and Citrine signals for PPM2, PPMC5, PPMC6, and PpMADS-S were observed in archegonia (Figs. 10d and 11e). The specific archegonium cells displaying the signals varied depending on the gene. GUS signals for PpMADS-S were detected at the base of antheridia but were not detected at the base of old antheridia that had released their sperm (Fig. 10d). After fertilization, the zygote divides to form a sporophyte stem cell, and subsequent cell divisions form the sporophyte body, including a sporangium, in which spores are produced after meiosis. The spatiotemporal localization of the six proteins varied, with partial overlap, during sporophyte development (Figs. 10e and 11f). In total, the localization of the Physcomitrella MIKC^{C}-type MADS-domain proteins differ and that at least one MIKC^{C}-type MADS-domain protein is detected in most tissue of Physcomitrella.

4.2. MIKC^{C}-type MADS-box genes negatively regulate cell divisions and growth in the gametophore stem

To analyse the roles of the six MIKC^{C}-type MADS-box genes, single deletion mutant

lines for each gene were produced using homologous recombination (Figs. 5 and 6). As previously reported (Singer et al., 2007), single deletion mutants *ppm1*, *ppm2,* and *ppmads1* were indistinguishable from the wild type (Fig. 13). Similarly, any phenotypic differences between single deletion mutants of the other three genes and the wild type was not found throughout the lifecycle (Fig. 13). These observations were confirmed in two independent transgenic lines for each gene. Since the protein localization of the six genes were found to partially overlap in time and space, all six MIKC^{C}-type MADS-box genes were deleted to form sextuple deletion mutant lines using homologous recombination (Figs. 5 and 6).

Two sextuple deletion mutant lines independently generated from different quintuple deletion mutant lines (*ppm1 ppm2 ppmads1 ppmc5 ppmc6 ppmads-s* #109 and *ppm1 ppm2 ppmads1 ppmc5 ppmc6 ppmads-s* #305) were analysed, and both lines showed the same phenotypes. Following observations and experiments were repeated at least three times. The wild type and the sextuple deletion mutants were observed throughout the lifecycle (Fig. 14a–e). Whereas the chloronemata and caulonemata of the sextuple deletion mutant lines were indistinguishable from those of the wild type (Fig. 14a,b), the gametophores of the sextuple deletion mutant lines were taller and had longer internodes than the wild type (Fig. 14c,f), and the number and length of cells in each internode were significantly increased in the sextuple mutant lines compared with the wild type (Fig 14g,h). These indicate that MIKC^{C}-type MADS-box genes negatively regulate cell division and growth in gametophore internodes. To investigate genes targeted by the MADS-box genes, the gametophore transcriptomes of the wild type and sextuple deletion mutant line #109 were compared. The transcript levels of 322 and 152 genes were increased and decreased in the mutant, respectively, compared with those of

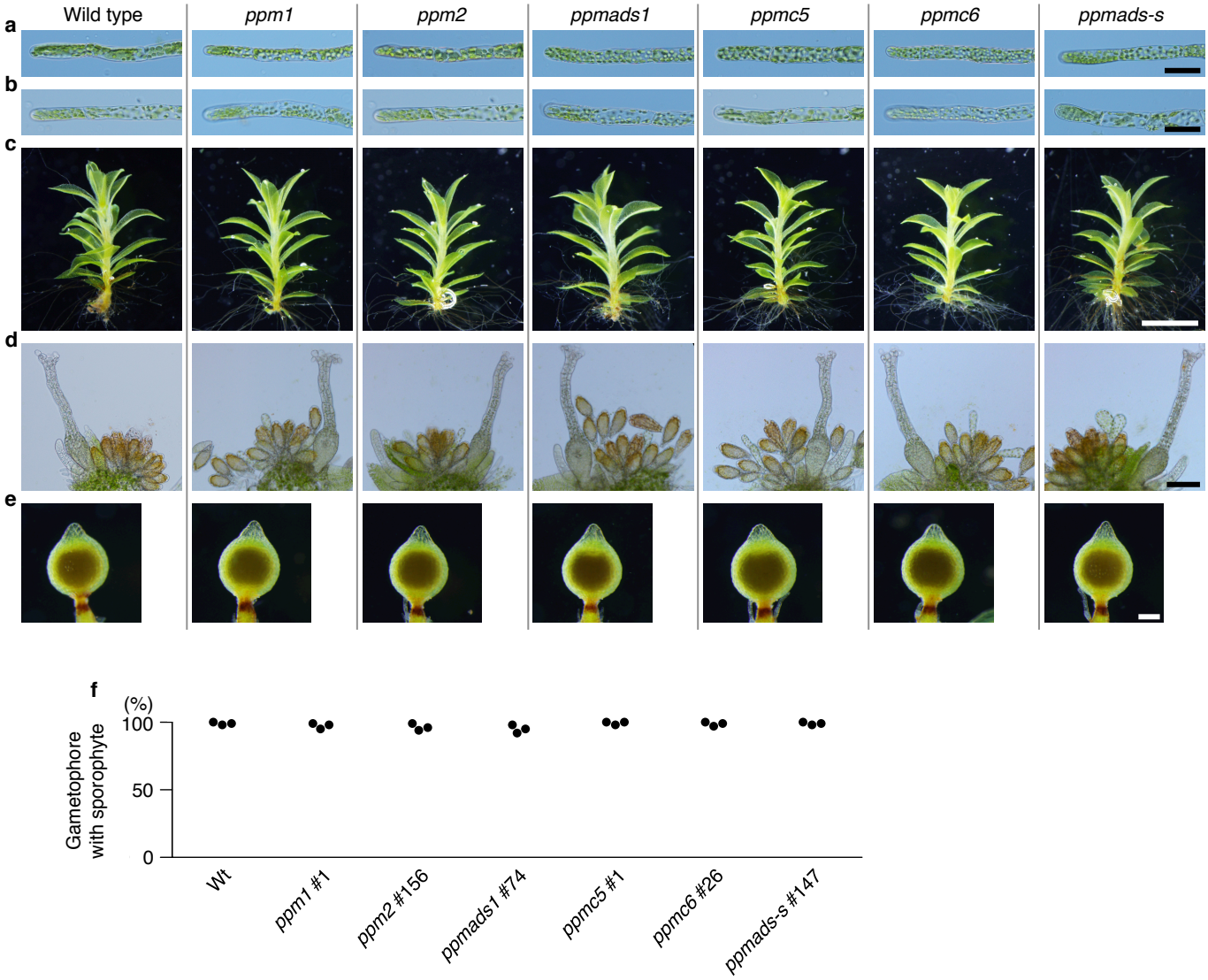

Figure 13 | Morphological analyses of the single deletion mutant lines of each of the six MIKC^{C}-type MADS-box genes. a–e, Representative images of the chloronema filaments (**a**), caulonema filaments (**b**), gametophores (**c**), antheridia and archegonia (**d**), and sporophytes (**e**) in the wild type, *ppm1* mutant line #1, *ppm2* mutant line #156, *ppmads1* mutant line #74, *ppmc5* mutant line #1, *ppmc6* mutant line #26, and *ppmads-s* mutant line #147. **f**, Percentages of gametophores forming at least one sporophyte in the wild type and the single mutant lines described in **a–e**. Scale bars, 50 µm in **a**,**b**,**e**; 2 mm in **c**; 100 µm in **d**.

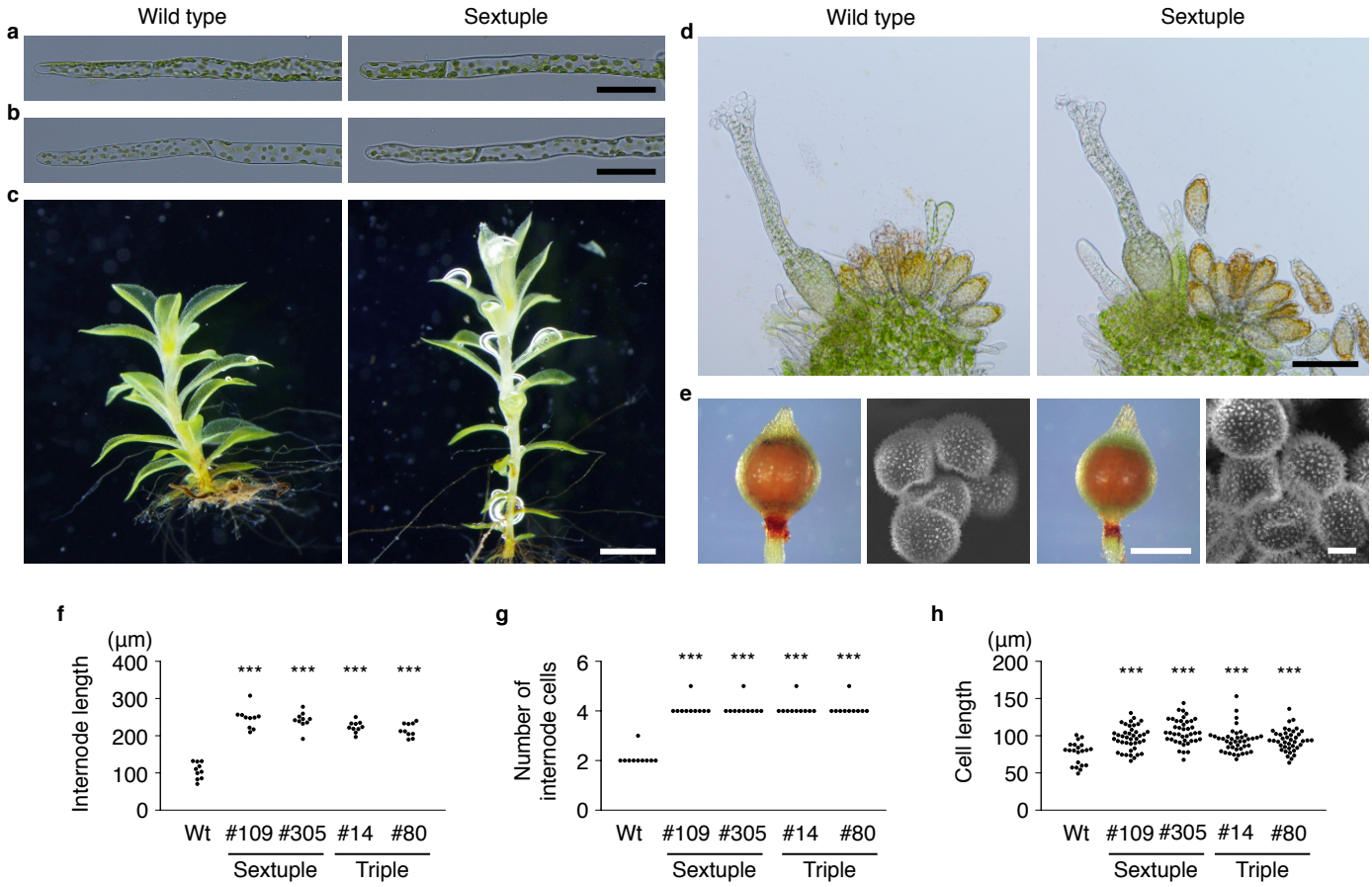

Figure 14 | Morphological comparisons between the wild-type and deletion mutant lines. a–e, Representative images of the chloronema filaments (**a**), caulonema filaments (**b**), gametophores (**c**), antheridia and archegonia (**d**), sporophytes and spores (**e**) in the wild type and the sextuple deletion mutant line #109. **f–h**, Length of gametophore internodes (**f**), the number of cells per internode (**g**), and length of cells per internode (**h**) in the wild type, the sextuple mutant lines #109 and #305, and the *ppm1 ppm2 ppmc6* triple deletion mutant lines #14 and #80. *** $p < 0.001$ by two-tailed Dunnett test for multiple comparisons (n = 10 gametophores per line [**f**,**g**] and n = 21, 41, 41, 41, and 41 cells of ten internodes in the wild type, the sextuple mutant line #109, the sextuple mutant line #305, the triple deletion mutant line #14, and the triple deletion mutant line #80, respectively [**h**]). Scale bars, 50 µm in **a**,**b**; 1 mm in **c**; 100 µm in **d**; 500 µm (sporophyte) and 10 µm (spore) in **e**.

the wild type. To investigate which genes are similarly regulated by MIKC^{C}-type MADS-box genes in Physcomitrella and *Arabidopsis thaliana* (Arabidopsis), the Arabidopsis putative orthologs of the Physcomitrella differently expressed genes (DEGs) to the Arabidopsis DEGs identified in comparisons between the wild type and mutants of MIKC^{C}-type MADS-box genes *APETALA1* (*AP1*; Kaufmann et al., 2010), *APETALA3* (*AP3*; Wuest et al., 2012), *PISTILLATA* (*PI*; Wuest et al., 2012), *AGAMOUS* (*AG*; Maoiléidigh et al., 2013), *SUPPRESSOR OF OVEREXPRESSION OF CO 1* (*SOC1*; Seo et al., 2009; Tao et al., 2012), and *SHORT VEGETATIVE PHASE* (*SVP*; Gregis et al., 2013) were compared. A total of 25 of the 1,392 DEGs in the *AP1* over-expressor, 9 of the 1,075 *ap3* DEGs, 26 of the 1,471 *pi* DEGs, 16 of the 1,047 *ag* DEGs, 24 of the 1,209 *soc1* DEGs, and 25 of the 1,381 *svp* DEGs were the Arabidopsis orthologs of the Physcomitrella DEGs (Fig. 15), suggesting that these gene comprise candidates to be commonly regulated by MIKC^{C}-type MADS-box genes in both Arabidopsis and Physcomitrella.

To further examine the role of MIKC^{C}-type MADS-box genes in gametophore growth, inducible lines were generated for each of the six Physcomitrella MIKC^{C}-type MADS-box genes using the β-estradiol induction system (Kubo et al., 2013) (Fig. 7). Morphology of all lines without induction was not distinguished from that of wild type. Increased expression of *PPM1*, *PPM2*, or *PPMC6* caused shorter gametophore internodes than those in the uninduced plants, but increasing the expression of the other genes did not (Fig. 16). *PPM2* over-expression also resulted in spicate gametophores and fewer rhizoids than in the controls. These morphological changes are concordant with the gametophore expression of *PPM1*, *PPM2*, and *PPMC6* genes (Figs. 10c and 11c). To examine whether internode length is regulated by these

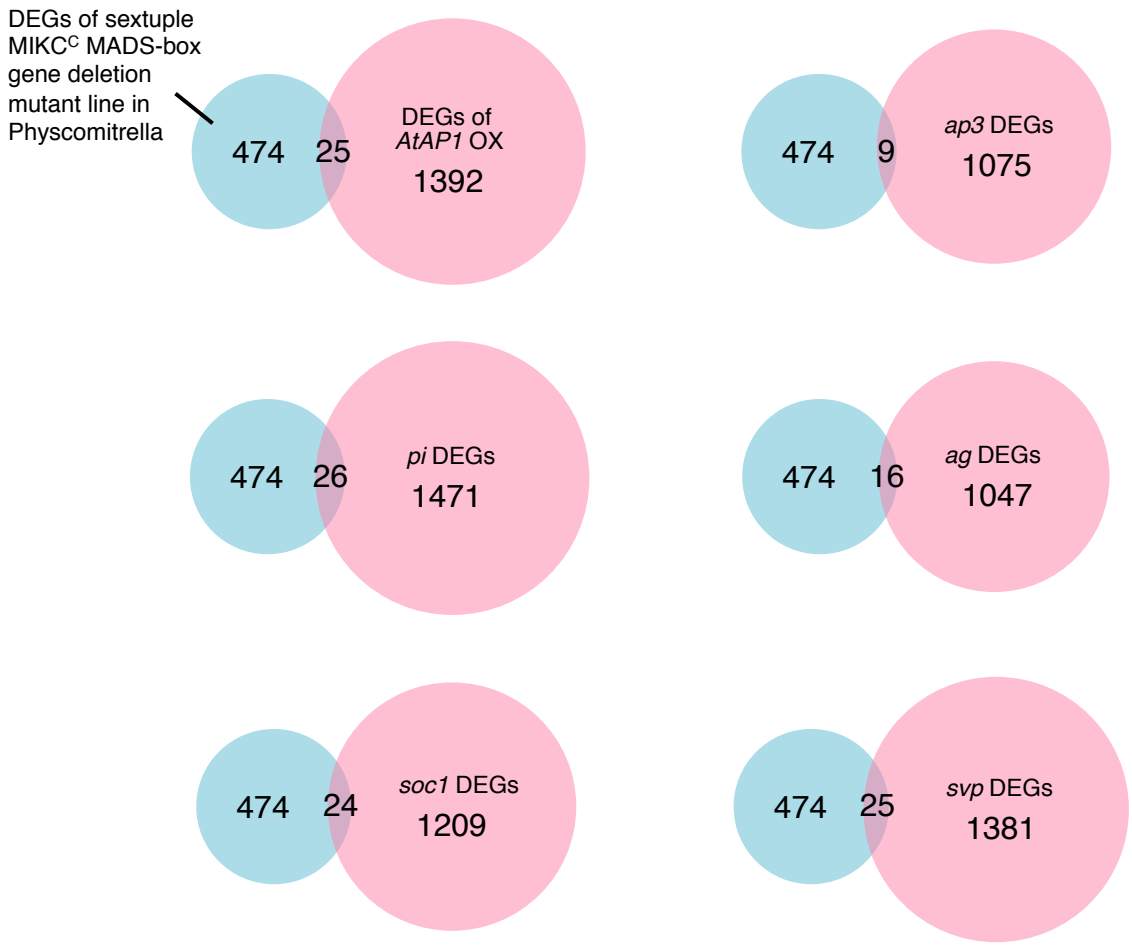

Figure 15 | Venn diagrams of differently expressed genes (DEGs) in MIKC^C-type MADS-box gene mutants in Physcomitrella and Arabidopsis. The blue circles represent the number of Arabidopsis orthologs of DEGs identified in comparisons between the wild type and sextuple deletion mutant line #109 in Physcomitrella gametophore. The pink circles represent the number of DEGs identified in comparisons between the wild type and mutants of Arabidopsis MIKC^C-type MADS-box genes *AP1* (Kaufmann et al., 2010), *AP3* (Wuest et al., 2012), *PI* (Wuest et al., 2012), *AG* (Maoiléidigh et al., 2013), *SOC1* (Seo et al., 2009; Tao et al., 2012), and *SVP* (Gregis et al., 2013). The intersections represent the number of overlapped Arabidopsis orthologs of DEGs in Physcomitrella and Arabidopsis.

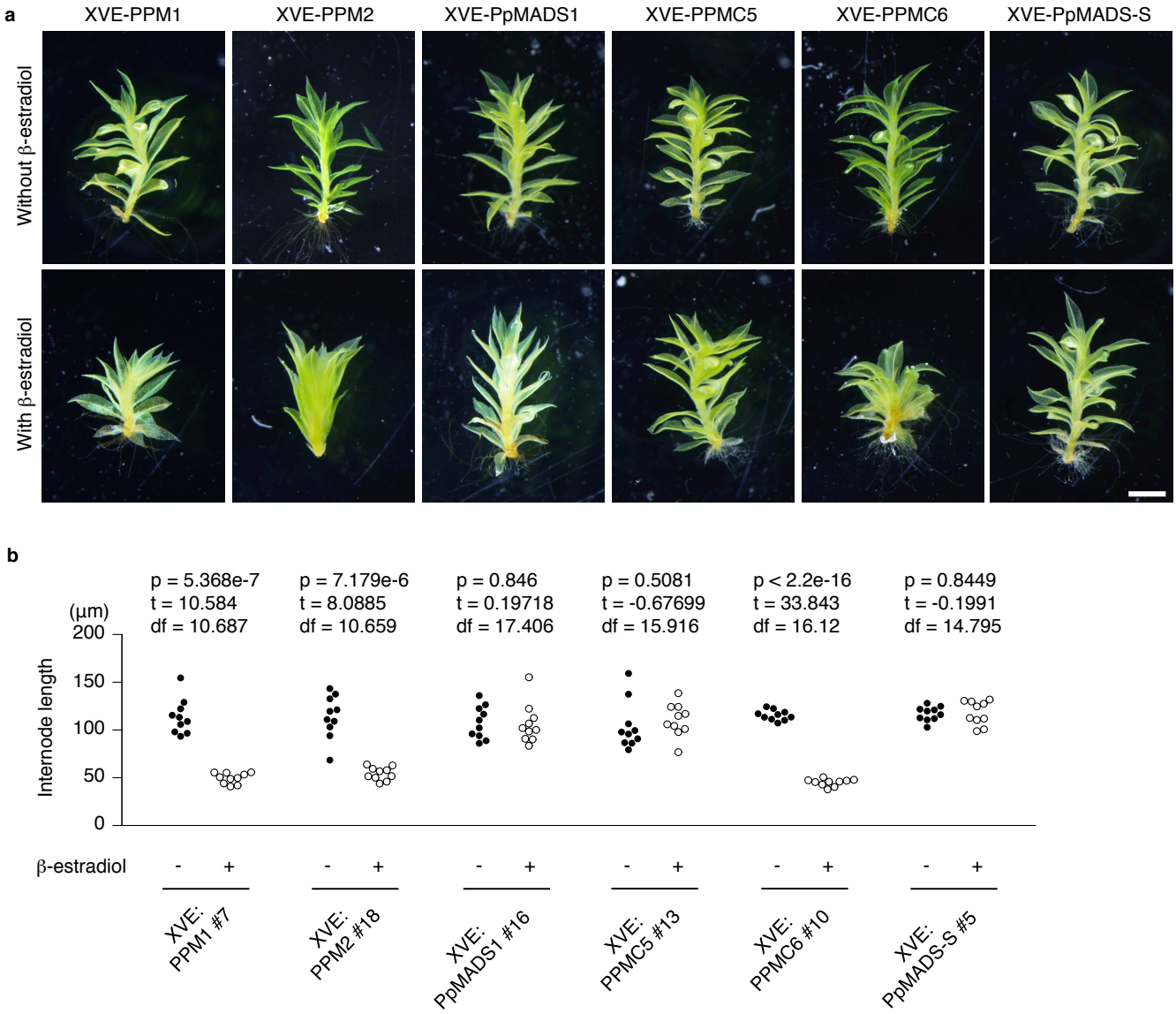

Figure 16 | Comparisons of gametophores from the wild-type and over-expression lines generated using the β-estradiol MIKC^{C}-type MADS-box gene induction system. a, Over-expression lines of each inducible MIKC^{C}-type MADS-box gene cultured with or without β-estradiol. **b**, Internode length of gametophores in the wild-type and over-expression lines. Statistical analyses were conducted using a two-tailed Welch's t-test (n = 10). p, p-value; t, t-value; df, degrees of freedom. Scale bar, 1 mm in **a**.

three genes, triple deletion mutant lines of *PPM1*, *PPM2*, and *PPMC6* were produced. The internode lengths of the triple deletion mutant lines were longer than the wild type, reaching the same lengths as the sextuple deletion mutant lines (Fig. 14f–h). Since single deletion mutant lines did not display the longer internode phenotype, this suggests that *PPM1*, *PPM2*, and *PPMC6* redundantly regulate cell division and growth in gametophore stems. To confirm the redundant functions of three genes, double deletion mutant lines (*ppm1 ppm2*, *ppm1 ppmc6*, and *ppm2 ppmc6*; Figs. 5 and 6) were produced. The internode lengths of the double deletion mutant lines were intermediate between those of wild type and the triple deletion mutant lines (Fig. 17a).

4.3. External water conduction is defective in the deletion mutant lines

In addition to the height change, the surface of the sextuple mutant gametophores looked drier than those of the wild type under the same culture conditions (Fig. 18a). When gametophores were submerged in water, more air bubbles were trapped on the mutant gametophores than on those of the wild type, which may be related to their dry surface (Fig. 14c). Mosses have both internal and external water conduction systems (Proctor, 2008), and the water on the surface of gametophores is supplied by the latter. External water conduction is mediated by capillary structures, the spaces within concave gametophore leaves and their basal sheaths (Proctor, 2008). To investigate external water conduction in the wild type and the sextuple deletion mutants, the base of a gametophore with leaves was put in a 1% Evans blue solution. The solution travelled up the wild-type gametophores at a speed of 4.47±0.55 mm s^{-1} (mean ± SE; n = 5) (Fig. 18b), but did not travel up the sextuple deletion mutant gametophores (Fig. 18b), indicating a defect in the external water conduction of the sextuple deletion mutant

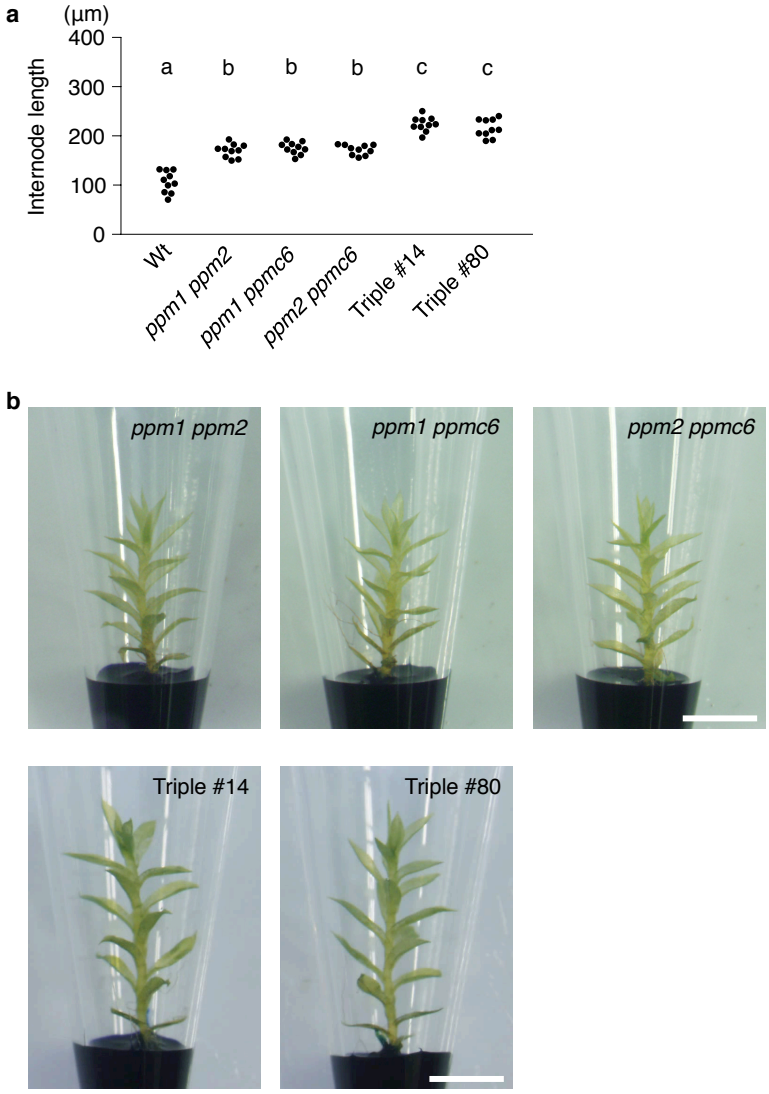

Figure 17 | Internode length and visualization of external water conduction in the double and triple deletion mutant lines. a, Length of gametophore internodes in the wild type, the *ppm1 ppm2* double deletion mutant line #1, the *ppm1 ppmc6* double deletion mutant line #9, the *ppm2 ppmc6* double deletion mutant line #2, and the *ppm1 ppm2 ppmc6* triple deletion mutant lines #14 and #80. Different letters indicate statistically significant differences by two-tailed Dunnett test for multiple comparisons ($p < 0.001$, $n = 10$ gametophores per line). **b**, Visualization of external water conduction using Evans blue solution in the *ppm1 ppm2* double deletion mutant line #1, the *ppm1 ppmc6* double deletion mutant line #9, the *ppm2 ppmc6* double deletion mutant line #2, and the *ppm1 ppm2 ppmc6* triple deletion mutant lines #14 and #80. Scale bars, 2 mm in **b**.

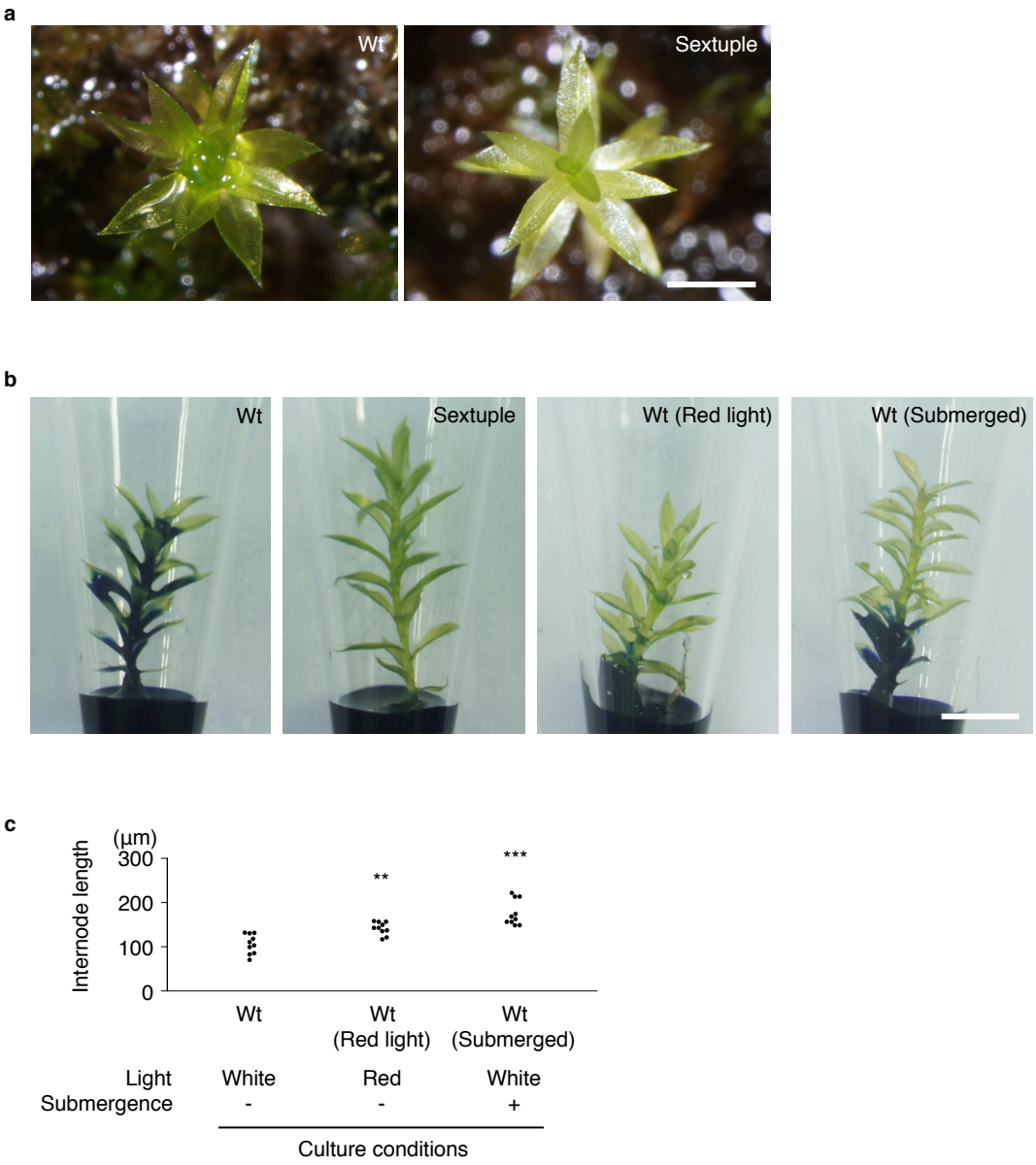

Figure 18 | Effects of the elongated internodes on the defects in external water conduction. a, Gametophores of the wild type and the sextuple deletion mutant line #109 cultivated under regular conditions. **b**, Visualization of external water conduction using Evans blue solution in the wild type cultivated under regular (white-light and non-submerged) conditions (Wt), the sextuple mutant line #109 under regular conditions (Sextuple), the wild type under red-light and non-submerged conditions (Wt [Red light]), and the wild type under white-light and submerged conditions (Wt [Submerged]). **c**, Length of wild-type gametophore internodes grown under the different conditions. ** $p < 0.01$; *** $p < 0.001$, two-tailed Dunnett test for multiple comparisons ($n = 10$). Scale bars, 1 mm in **a**; 2 mm in **b**.

lines. The defect was observed also in *ppm1 ppm2 ppmc6* triple deletion mutant lines as well as *ppm1 ppm2*, *ppm1 ppmc6*, and *ppm2 ppmc6* double deletion mutant lines (Fig. 17b).

There were two possibilities for this defect. The first was that the decreased wettability was caused by accumulated hydrophobic wax in the deletion mutant lines. To examine whether extra cuticular wax accumulates in the sextuple mutant gametophores to prevent capillary water movement, the surface structures of the stems and gametophore leaf bases (Fig. 19a,c), which are passages for capillary water (Fig.19b), were observed with transmission electron microscopy (TEM). The cuticles of the sextuple deletion mutant lines contained electron-dense structures (arrows in Fig. 19c) and were thicker on the middle part of the gametophore leaf blades, but not on the stem or gametophore leaf edges, compared to the wild type (Fig. 19d). The expression of certain genes involved in acyl-lipid metabolism (Li-beisson et al., 2013) increased in the mutant (Table 2), although the loads of wax esters with 45 to 56 carbon chain lengths were not different between the wild type and the mutant (Fig. 20). These data suggest that the electron-dense structures and thicker cuticle in the middle part of the gametophore leaf blades are caused by small, undetectable changes in the wax esters or changes in other lipids. Since external water is transmitted along the stems and gametophore leaf edges (Fig. 19b), the changes to the cuticle in the centre of the gametophore leaf blades are unlikely to be a major cause of the defects in external water conduction.

Another possibility is that the defect in capillary water transmission between gametophore leaves is caused by the elongated gametophore internodes in the sextuple deletion mutant lines. Water accumulates at a gametophore leaf axil until the droplet is

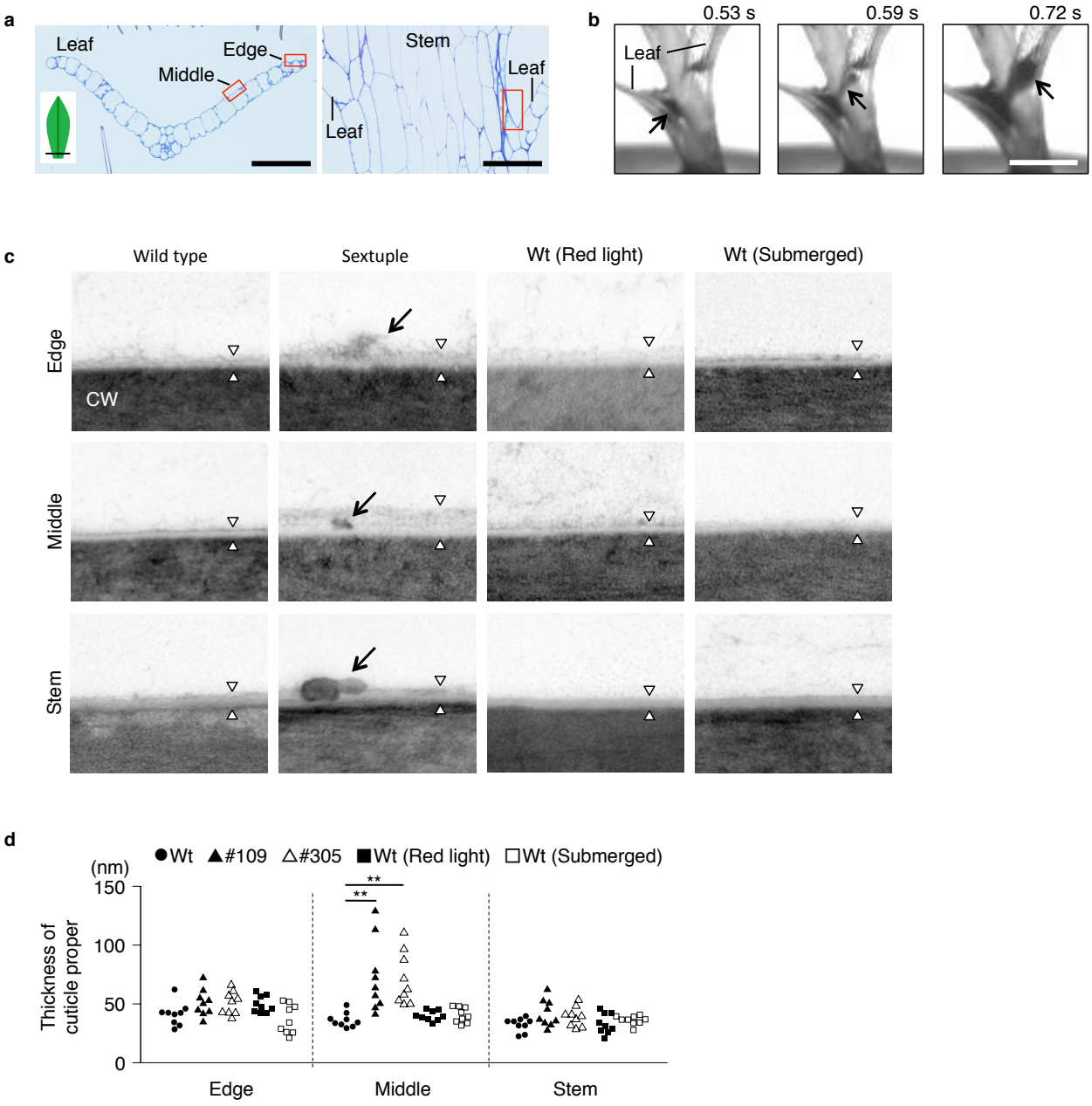

Figure 19 | Comparisons of the cuticle in the stems and gametophore leaf bases. a, Transverse sections of the basal part of a leaf (left) and longitudinal sections of a stem (right) observed using light microscopy. The approximate position of leaf sectioning is indicated in an inset. Red squares show the approximate areas observed using TEM. **b**, External water conduction in the wild type. Evans blue solution accumulates at a leaf axil (left), adheres to the narrow space between a stem and the base of a leaf directly above (centre), and accumulates in the leaf axil (right). Arrows indicate approximate fronts of Evan blue solution. Time after putting the gametophore base in the solution is indicated in seconds above the images. **c**, TEM images of sections of the leaf edge (left), the central leaf area between an edge and a midvein (centre), and a stem (right) of gametophores cultivated under the conditions described in **a**. CW, cell wall. Arrows indicate electron-dense structures. Arrowheads indicate the cuticle proper. **d**, Thickness of the cuticle proper. ** $p < 0.01$, two-tailed Dunnett test for multiple comparisons ($n = 9$). Scale bars, 100 µm in **a**; 0.5 mm in **b;** 100 nm in **c**.

Table 2. Certain genes involved in acyl-lipid metabolism increased in the sextuple deletion mutant line #109.

Physcomitrella gene ID	Best hit Arabidopsis gene ID*	Symbol†	Description†	Fold change	Q-value
Phpat.001G114200	AT4G25140.1	OLE1, OLEO1	oleosin 1	7.8	2.21E-12
Phpat.006G008200	AT2G33380.1	CLO-3, RD20	Caleosin-related family protein	7.38	1.11E-08
Phpat.010G094200	AT3G06060.1	n.a.	NAD(P)-binding Rossmann-fold superfamily protein	5.9	1.23E-24
Phpat.013G032600	AT3G11170.1	FAD7, FADD	fatty acid desaturase 7	3.07	2.67E-10
Phpat.016G086200	AT3G02600.1	ATLPP3, LPP3	lipid phosphate phosphatase 3	3.02	7.50E-07
Phpat.019G038400	AT3G51520.1	n.a.	diacylglycerol acyltransferase family	2.8	6.99E-09
Phpat.023G002300	AT5G55240.1	ATPXG2	ARABIDOPSIS THALIANA PEROXYGENASE 2	2.63	2.62E-06
Phpat.011G083300	AT3G07400.1	n.a.	lipase class 3 family protein	2.01	0.000178458

*Obtained via Phytozome (DOE-JGI, https://phytozome.jgi.doe.gov/) as the top result of the BLASTP search to the Arabidopsis protein database using the corresponding Physcomitrella protein as a query.

†Information according to the annotation to the best hit Arabidopsis gene ID.

n.a.: not annotated

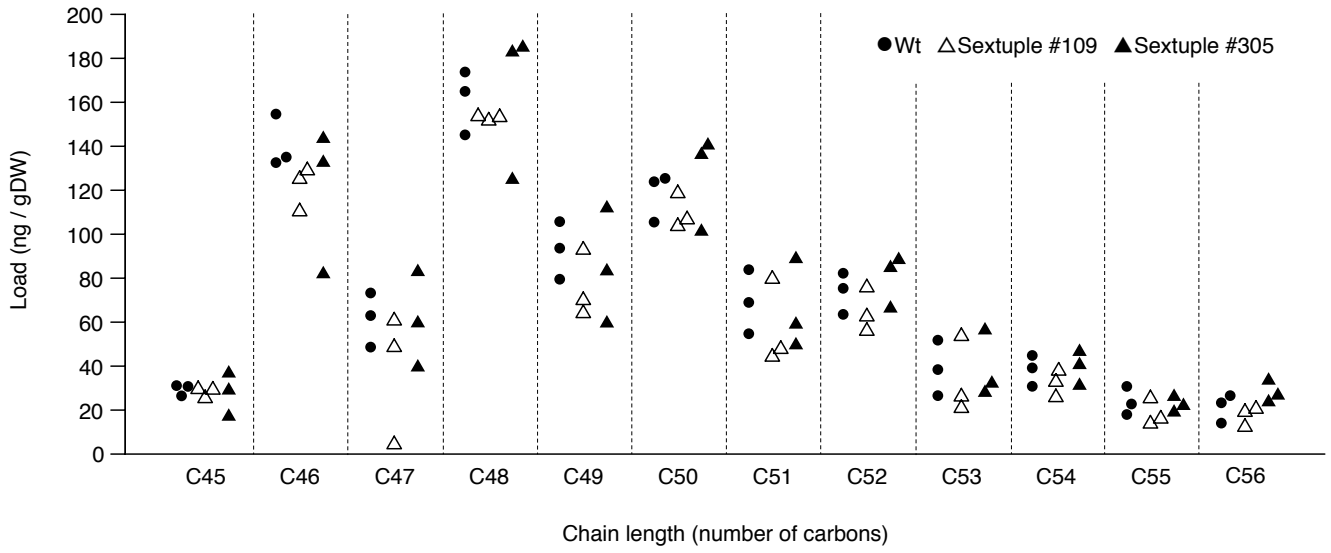

Figure 20 | Comparisons of the wax ester composition among wild-type and sextuple deletion mutant gametophores. Wax esters, the major molecular species of extracellular lipids in *Physcomitrella patens* (Buda et al., 2013), were quantified using gas chromatography-flame ionization detection. Closed circles, open triangles and closed triangles indicate wax ester contents in the wild type and sextuple mutant lines #109 and #305, respectively.

large enough to touch the axil immediately above, then it is sucked to the upper axil by capillary action, driven by the narrow space between the adaxial leaf surface and the stem surface facing it (Fig. 19b). To investigate the effect of internode length on external water conduction in a single genetic background, wild-type gametophores cultivated under regular conditions were moved to red-light or submerged conditions to elongate the stems (Imaizumi et al., 2002) (Fig. 18c). In contrast to the sextuple deletion mutant lines, the cuticles of wild-type gametophore leaves and stems were indistinguishable between the different culture conditions (Fig. 19c,d). Nevertheless, Evans blue solution travelled up the stems of gametophores in which the basal gametophore leaves formed under regular conditions, but did not travel up to the elongated parts formed under the subsequent red-light or submerged conditions (Fig. 18b). These results indicate that the defect in external water conduction is caused by elongated internodes even in the absence of visible changes to the cuticle.

4.4. Sperm entry into archegonia is less efficient in the deletion mutant lines

When gametophores of the sextuple deletion mutant lines were grown under short-day conditions at 15ºC for three weeks (Sakakibara et al., 2008), antheridia and archegonia were formed at the tops of gametophores, and sporophytes formed after fertilization. The outer morphology of the antheridia, archegonia, sporophytes, and spores in the mutant lines were indistinguishable from those in the wild type (Fig. 13d,e); however, the percentage of gametophores forming sporophytes significantly decreased in the mutants (Fig. 21a). Since bryophytes need water for sperm to swim to the archegonia for fertilization, it was hypothesized that the shortage of water around the gametangia caused by the defect in external water conduction impaired fertilization. The number of

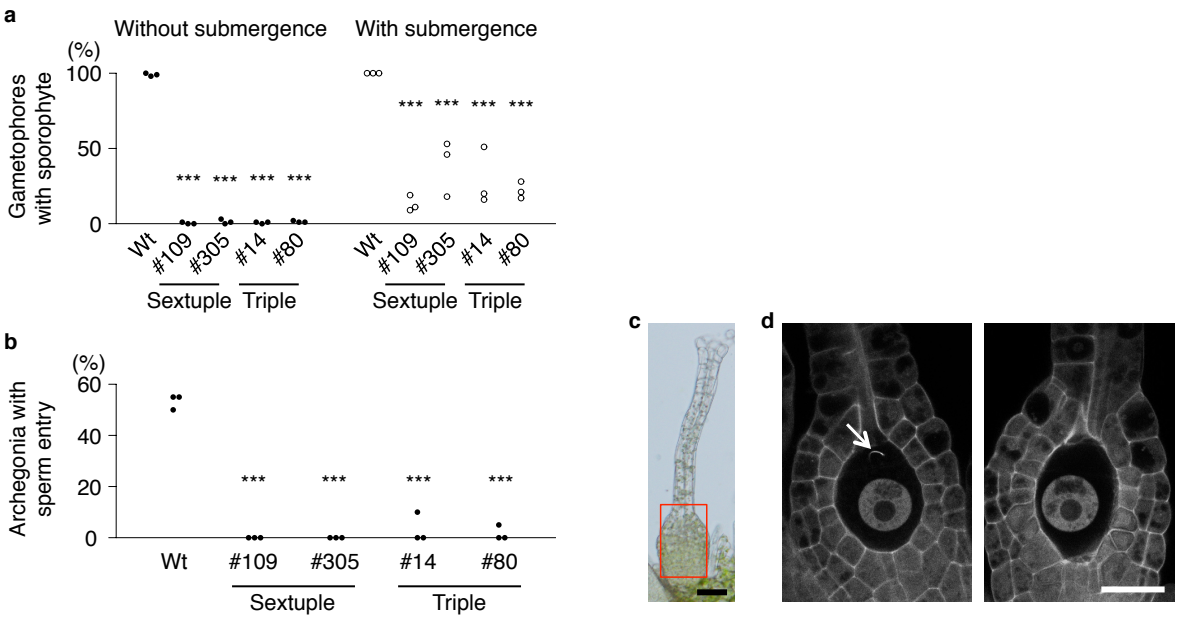

Figure 21 | Frequency of sporophyte formation by gametophores and percentages of archegonia with sperm entry in the wild-type and the deletion mutant lines. a,**b**, Percentages of gametophores with at least one sporophyte (**a**) and those of archegonia with sperm entry (**b**) in the wild type, the sextuple mutant lines #109 and #305, and the *ppm1 ppm2 ppmc6* triple deletion mutant lines #14 and #80. In each of three experiments, 100 gametophores (**a**) and 20 archegonia (**b**) were examined. *** $p < 0.001$ by two-tailed Dunnett test for multiple comparison (triplicates of n = 100 gametophores [**a**] and triplicates of n = 20 archegonia [**b**]). **c**,**d**, Archegonia (**c**) with (left) or without (right) sperm (arrow) entry were observed by confocal microscopy (**d**). The red square in **c** indicates the approximate area shown in **d**. Scale bars, 50 μm in **c**; 20 μm in **d**.

archegonia into which sperm entered was decreased in the sextuple deletion mutant lines compared with the wild type (Fig. 21b-d). Furthermore, when water was supplied to the gametangia by submerging them at the time of fertilization, the number of sporophytes increased (Fig. 21a). These findings indicate that the lack of water for fertilization is one of the reasons for the reduced number of sporophytes produced in the sextuple deletion mutants.

4.5. MIKC^{C}-type MADS-box proteins regulate genes involved in flagellum formation

Since the water supply did not completely complement the reduced number of sporophytes in the sextuple deletion mutant lines (Fig. 21a), the viability of the sperm and eggs was examined as next. The *pplfy1 pplfy2* double deletion mutant line is defective in zygote cell division and does not form any normal sporophytes, while almost all wild-type gametophores form sporophytes (Tanahashi et al., 2005). When the *pplfy1 pplfy2* double deletion mutant line and the wild type were cultivated in the same plastic box and submerged in water for crossing, the percentage of gametophores producing normal sporophytes increased in the *pplfy1 pplfy2* mutant (6.8 ± 1.1% [mean ± SE; n = 100 gametophores for each of 10 crosses]), likely because of the crossing between *pplfy* egg cells and wild-type sperm. Crosses between the *pplfy1 pplfy2* line and the wild type result in fewer gametophores with sporophytes on the *pplfy1 pplfy2* line compared self-crosses of the wild type (Himi et al., 2001), likely because of the low efficiency of crossing. By contrast, the crossing between the sextuple deletion mutant line and the *pplfy* double deletion mutant line resulted in fewer sporophytes on the *pplfy* gametophores (0.5 ± 0.3% [mean ± SE; n = 100 gametophores for each of 10 crosses])

than when they were crossed with the wild type. This suggests that the sextuple deletion mutant line has a defect in sperm. To investigate egg cell viability, the sextuple deletion mutant line was crossed with the wild type. The number of sporophytes in the mutant lines increased (26.3 ± 2.2% [mean ± SE; n = 100 gametophores for each of 10 crosses]), indicating that egg cells of the mutant lines are functional.

To further investigate the defects of sperm in the sextuple deletion mutant lines, sperm movement and structures were observed. The two sperm flagella were observed using differential interference contrast microscopy, and those of the wild type and the sextuple mutants were indistinguishable (Fig. 22a,b). Using dark-field microscopy, the wild-type sperm swam using two flagella; one beating around the head of sperm for steering and the other beating towards the tail for propulsive force (Figs. 22c and 23), as observed in the liverwort *Marchantia polymorpha* (Miyamura et al., 2002). By contrast, the sperm of the sextuple deletion mutant did not swim as well as the wild-type sperm (Fig. 22d), and the percentage of sperm with moving flagella, the swimming speed, and the rotation frequency were all decreased in the sextuple deletion mutant lines (Fig. 22e–g).

To investigate whether the inferior movement was caused by structural defects in the flagella, their reactivation following the addition of exogenous ATP was measured with de-membraned isolated flagella. The reactivation rates of the mutant flagella were less than 5%, in comparison with approximately 20% in the wild-type flagella (Fig. 22h). This difference indicates that the mutant flagella have structural defects, although any differences between the sperm of the wild type and the sextuple deletion mutant lines were not detected in resin-embedded sections using TEM (Fig. 24). Since *PPM1*, *PPM2*, and *PPMC6* are expressed in the antheridia, the triple deletion

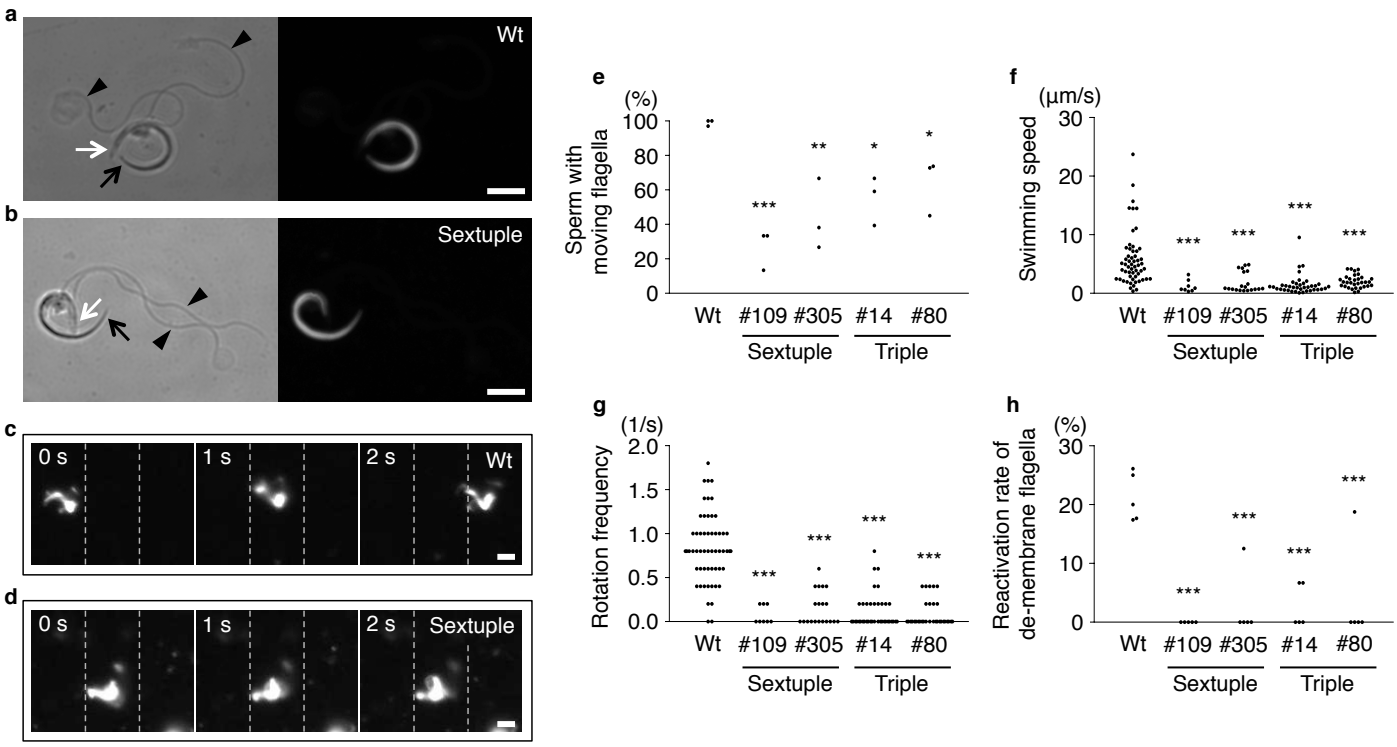

Figure 22 | Sperm movement is defective in the deletion mutant lines. a,**b**, Differential interference contrast images (left) and DAPI fluorescence images (right) of a sperm in the wild type (**a**) and the sextuple deletion mutant line #109 (**b**). White arrows, black arrows, and arrowheads indicate heads, tails, and flagella, respectively. **c**,**d**, Movement of sperm in the wild type (**c**) and the sextuple mutant line #109 (**d**) observed using dark-field microscopy. **e**, Percentages of sperm with moving flagella. * $p < 0.05$, ** $p < 0.01$, *** $p < 0.001$ by two-tailed Dunnett test for multiple comparisons (n = 57, 39, 63, 71, and 50 sperm in three antheridia of the wild type, the sextuple mutant line #109, the sextuple mutant line #305, the *ppm1 ppm2 ppm6* triple deletion mutant line #14, and the *ppm1 ppm2 ppm6* triple deletion mutant line #80, respectively). **f**,**g**, Swimming speed of sperm (**f**) and rotation frequency of the sperm body during swimming (**g**). *** $p < 0.001$ by two-tailed Dunnett test for multiple comparisons (n = 56, 8, 20, 38, and 32 sperm in three antheridia of the wild type, the sextuple mutant #109, the sextuple mutant #305, the triple deletion mutant #14, and the triple deletion mutant #80, respectively). **h**, Reactivation rates of de-membraned flagella following the exogenous addition of ATP. *** $p < 0.001$ by two-tailed Dunnett test for multiple comparisons (n = 89, 88, 85, 97, and 91 sperm of five antheridia in the wild type, the sextuple mutant #109, the sextuple mutant #305, the triple deletion mutant #14, and the triple deletion mutant #80, respectively). Scale bars, 5 μm in **a**–**d**.

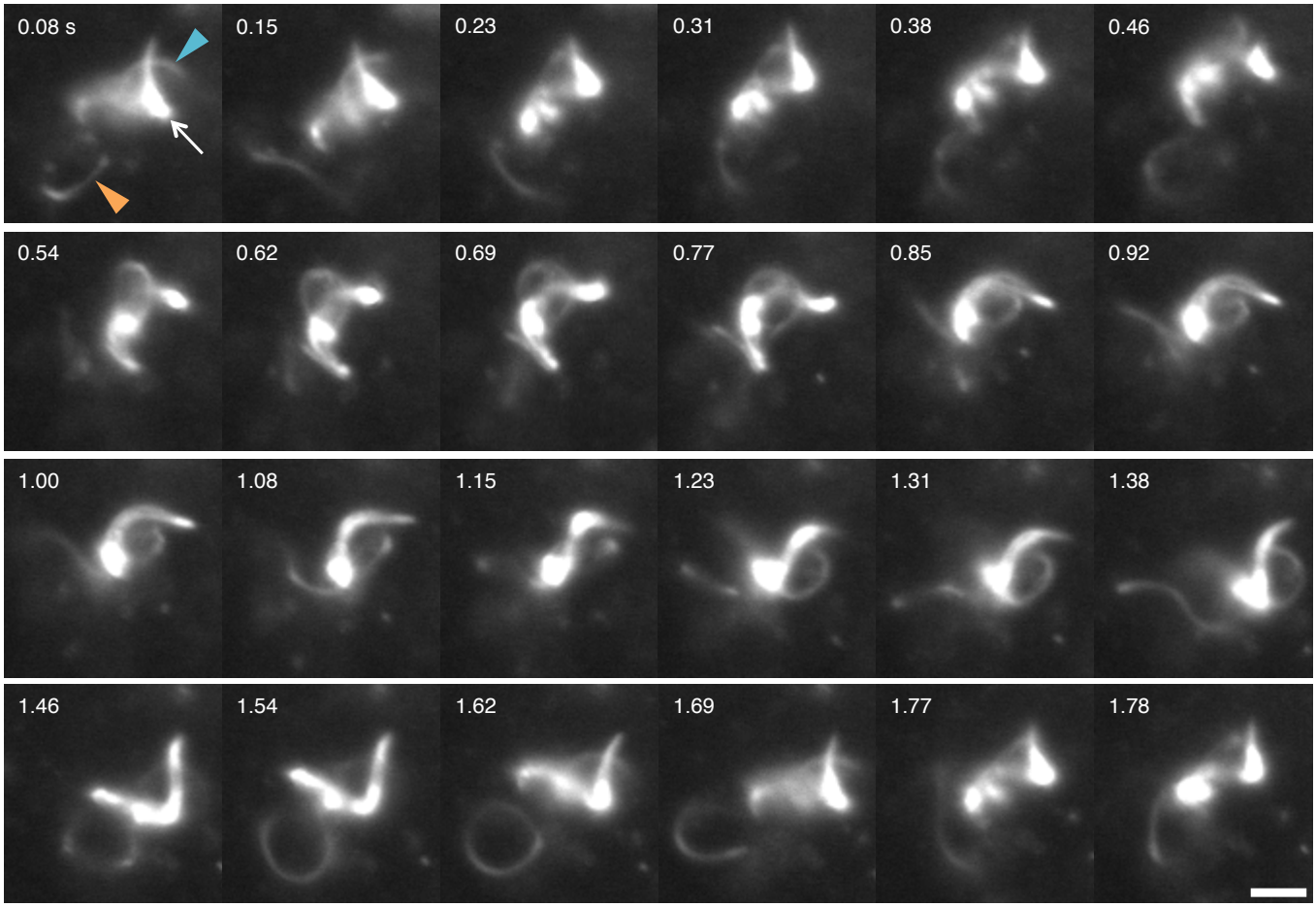

Figure 23 | Image sequence of the movement of a wild-type sperm observed using dark-field microscopy. An arrow indicates the elongated spiral sperm body and the aggregated nucleus. The blue arrowhead indicates a flagellum beating around the head of the sperm. An orange arrowhead indicates a flagellum elongating toward the tail and beating. Scale bar; 5 μm.

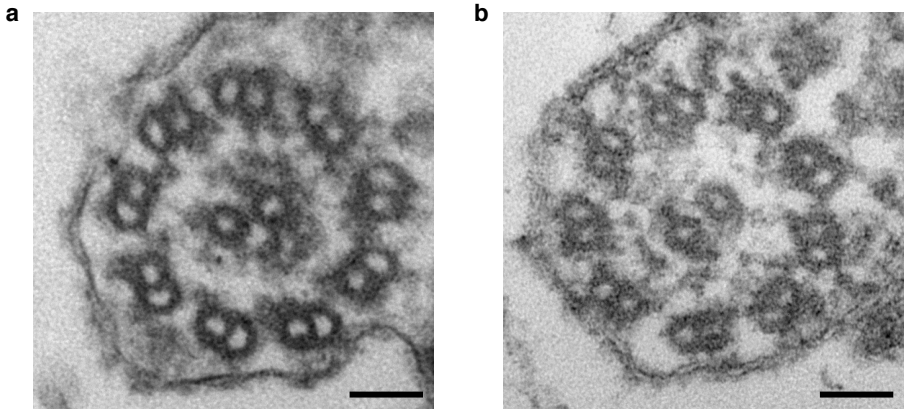

Figure 24 | Transmission electron micrographs of transverse sections of flagella in the wild type and a sextuple deletion mutant line. a,**b**, Transmission electron micrographs of transverse sections of a sperm flagellum from the wild type (**a**) and the sextuple mutant line #109 (**b**). Scale bars, 50 nm in **a**,**b**.

mutant lines were observed and similar defects were detected in sporophyte formation (Fig. 21a), the number of sperm in the archegonia (Fig. 21b), sperm movement (Fig. 22e–g), and the flagellum reactivation rates (Fig. 22h). None of the single deletion mutants of the three genes showed defects in sporophyte formation (Fig. 13f); therefore, *PPM1*, *PPM2*, and *PPMC6* appear to function redundantly to regulate flagellum motility. The *ppm1 ppm2*, *ppm1 ppmc6*, and *ppm2 ppmc6* double deletion mutant lines showed lower sperm motility than that of the wild type. The defects were close to or the same as those of the triple deletion mutant lines (Fig. 25a-c).

Next, the transcriptomes of the antheridia containing sperm in the sextuple deletion mutant line #109 and the triple deletion mutant line #14 with the wild type were compared. The transcript levels of 707 and 660 genes were increased and decreased in the sextuple mutant compared with the wild type, while 371 and 779 genes were increased and decreased in the triple mutant, respectively. The expression of 23 Physcomitrella genes orthologous to flagellum-related genes of the flagellate green algae *Chlamydomonas reinhardtii* (Pazour et al., 2005) were decreased in the both mutant lines (Table 3), further suggesting their involvement in the structural defects of the Physcomitrella flagella.

Over-expression lines of *PPM1*, *PPM2*, and, *PPMC6* were also observed (Fig. 26). Induction of *PPM1* caused approximately two days delayed formation of antheridia and archegonia, but the morphology was not different from that without induction (Fig. 26a). Induction of *PPM2* caused abnormal antheridia morphologies. Inner parts of antheridia became brown (a arrow in Fig. 26b) and outer cells of antheridia were expanded (arrows in Fig. 26c,e). In addition, elongated cells were observed at the shoot apex (arrows in Fig. 26f,g). Induced expression of *PPMC6* caused browned antheridia

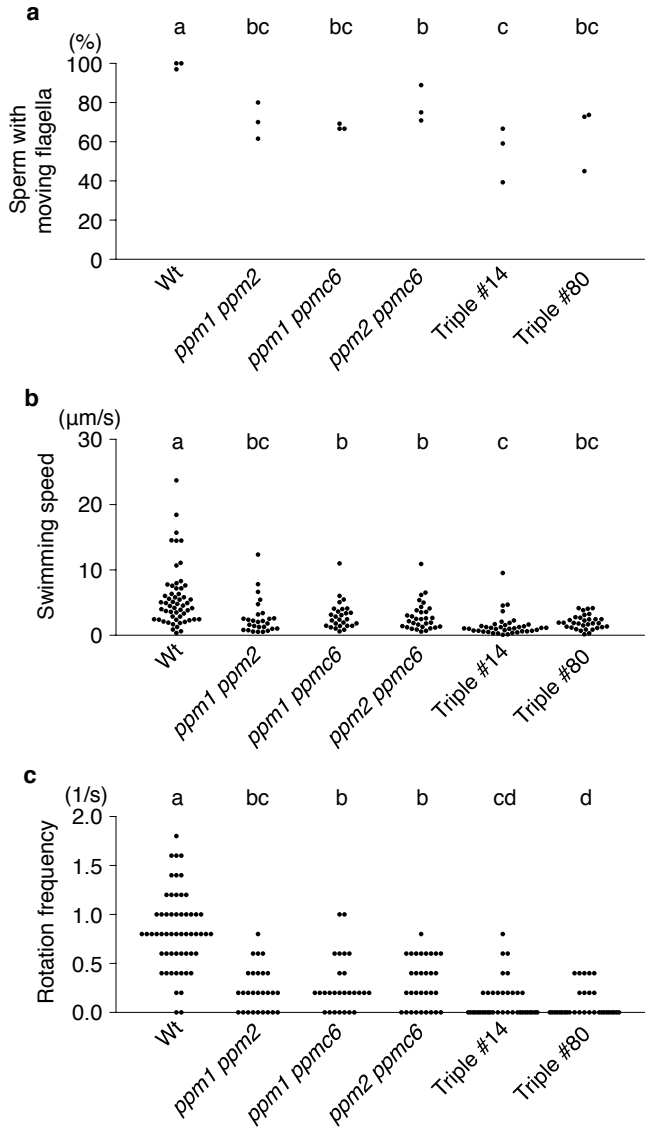

Figure 25 | Quantitative analyses of sperm movement in the wild type, the double deletion mutant, and the triple deletion mutant lines. a, Percentages of sperm with moving flagella. Different letters indicate statistically significant differences by two-tailed Dunnett test for multiple comparisons ($p < 0.05$, n = 57, 38, 40, 40, 71, and 50 sperm in three antheridia of the wild type, the *ppm1 ppm2* double deletion mutant line #1, the *ppm1 ppmc6* double deletion mutant line #9, the *ppm2 ppmc6* double deletion mutant line #2, and the *ppm1 ppm2 ppmc6* triple deletion mutant lines #14 and #80, respectively). **b**,**c**, Swimming speed of sperm (**b**) and rotation frequency of the sperm body during swimming (**c**). Different letters indicate statistically significant differences by two-tailed Dunnett test for multiple comparisons ($p < 0.05$, n = 56, 27, 27, 31, 38, and 32 sperm in three antheridia of the wild type, the *ppm1 ppm2* double deletion mutant line #1, the *ppm1 ppmc6* double deletion mutant line #9, the *ppm2 ppmc6* double deletion mutant line #2, and the *ppm1 ppm2 ppmc6* triple deletion mutant lines #14 and #80, respectively).

Table 3. Flagellum-related genes whose transcript levels decreased in both the sextuple mutant line #109 and the triple deletion mutant line #14.

Physcomitrella gene ID	Fold change*	Best hit Chlamydomonas gene ID†	Identity (%)‡	Symbol§	Description§	Best hit Arabidopsis gene ID‖	Identity (%)¶
Phpat.023G061600	3.15	Cre05.g244250	50.1	DHC6	Flagellar inner arm dynein heavy chain, dynein a (monomeric)	n.d.	-
Phpat.023G078700	2.98	Cre03.g190950	89.9	TUA1	Alpha tubulin 1	AT1G04820	89.7
Phpat.016G094100	2.33	Cre11.g476850	55.6	PF2, DRC4	Component of dynein regulatory complex	n.d.	-
Phpat.012G040900	2.33	Cre12.g511850	66.3	GSK3	Glycogen Synthase Kinase	AT5G14640	79.3
Phpat.013G037200	2.10	Cre03.g190950	89.2	TUA1	Alpha tubulin 1	AT1G04820	88.5
Phpat.009G087300	2.08	Cre02.g113400	53.6	BUG21	PARKIN COREGULATED GENE PROTEIN (1 of 1)	n.d.	-
Phpat.004G112100	2.05	Cre09.g393954	30.2	FAP106	n.a.	n.d.	-
Phpat.020G026800	2.02	Cre02.g141606	52.0	DHC9	Flagellar inner arm dynein heavy chain, dynein c (monomeric)	n.d.	-
Phpat.008G036400	1.95	Cre13.g607750	21.2	FAP250, DRC2	Flagellar Associated Protein	n.d.	-
Phpat.023G061100	1.93	Cre17.g698365	29.4	FAP172	n.a.	AT2G39690	24.6
Phpat.020G031100	1.91	Cre04.g217914	39.0	FAP57	Flagellar Associated Protein	AT5G14050	27.1
Phpat.015G043900	1.91	Cre06.g269950	84.3	CDC48, EZY21, NSG14	Protein involved in ubiquitin-dependent degradation of ER-bound substrates	AT5G03340	90.6

Phpat.008G010300	1.89	Cre12.g542250	94.7	RSP19, TUB1	Beta tubulin 1	AT5G62700	91.6
Phpat.006G102300	1.89	Cre09.g392282	58.3	DHC2	Dynein heavy chain 2, inner arm dynein d (monomeric)	n.d.	-
Phpat.017G007100	1.86	Cre09.g394251	52.9	PF16	Central pair associated protein	AT5G53480	40.0
Phpat.001G017400	1.86	Cre13.g567363	26.8	FAP220	n.a.	AT1G21980	36.6
Phpat.001G116400	1.83	Cre12.g502000	34.7	FAP253	Flagellar Associated Protein	n.d.	-
Phpat.019G006000	1.81	Cre12.g489750	49.7	FAP52	Flagellar Associated Protein	AT1G18080	30.6
Phpat.027G026000	1.81	Cre09.g392282	56.2	DHC2	Dynein heavy chain 2, inner arm dynein d (monomeric)	n.d.	-
Phpat.022G006800	1.78	Cre06.g268800	37.5	FAP60, FLA17, IFT139	Intraflagellar transport protein 139	AT4G12400	23.6
Phpat.015G016200	1.71	Cre09.g386750	79.1	HSP90A	Heat shock protein 90A	AT5G56000	84.2
Phpat.026G002900	1.71	Cre06.g299350	25.6	FBB15	Flagellar/basal body protein	AT1G55240	33.6
Phpat.013G013400	1.61	Cre06.g269950	86.8	CDC48, EZY21, NSG14	Protein involved in ubiquitin-dependent degradation of ER-bound substrates	AT5G03340	90.7

This list was made using known flagella-related genes in Chlamydomonas (Pazour et al., 2005).

[*]Obtained by comparison between the wild type and the sextuple deletion mutant line #109.

[†]Obtained via Phytozome (DOE-JGI, https://phytozome.jgi.doe.gov/) as the top result of the BLASTP search to the Chlamydomonas protein database using the corresponding Physcomitrella protein as a query.

[‡]Obtained by comparison between Physcomitrella proteins and best hit Chlamydomonas proteins.

[§]Information according to the annotation to the best hit Chlamydomonas gene ID.

[‖]Obtained via Phytozome (DOE-JGI, https://phytozome.jgi.doe.gov/) as the top result of the BLASTP search to the Arabidopsis protein database using the corresponding Physcomitrella protein as a query.

[¶]Obtained by comparison between Physcomitrella proteins and best hit Arabidopsis proteins.

n.a.: not annotated

n.d.: not detected

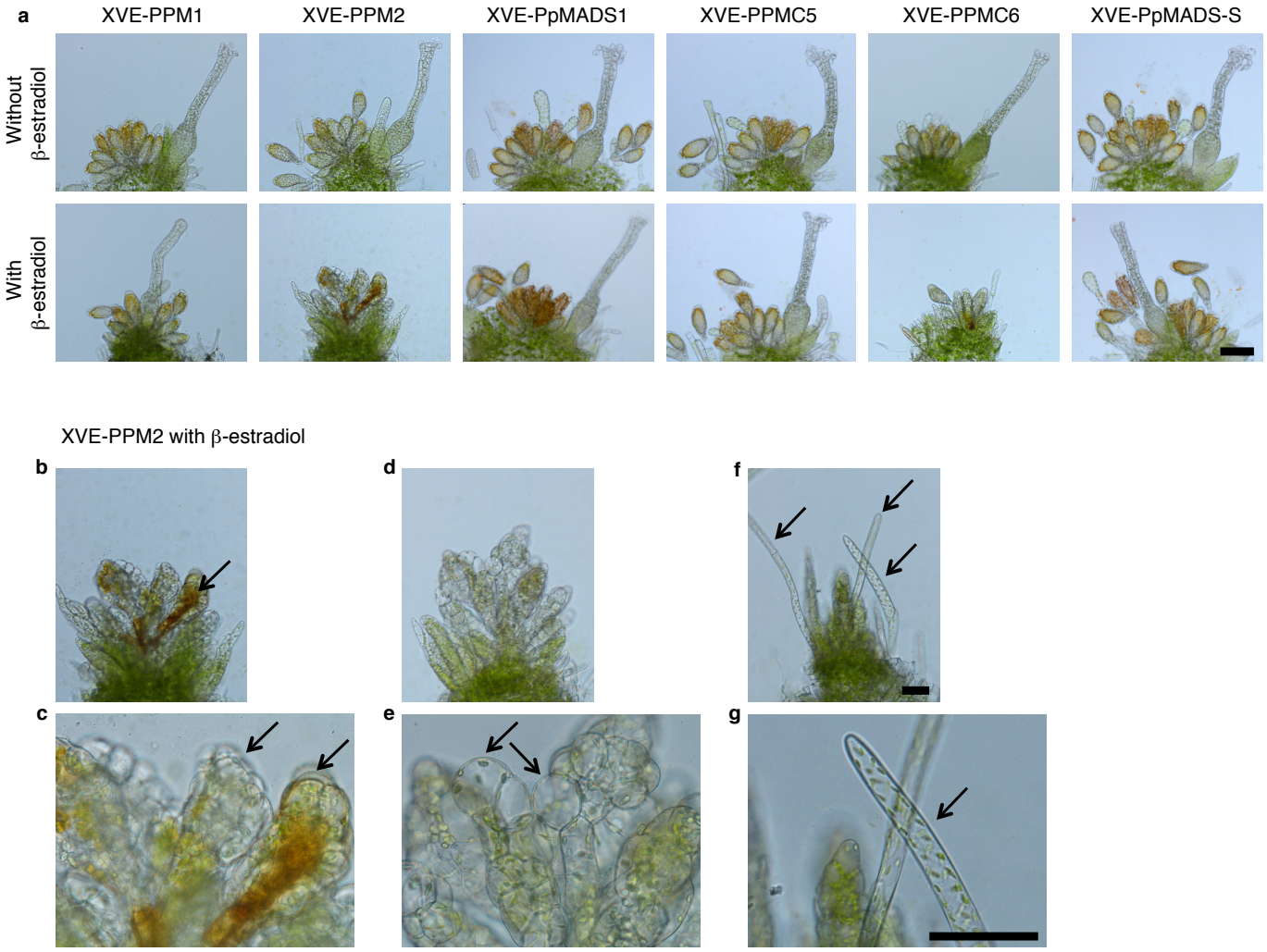

Figure 26 | Comparisons of gametangia from the over-expression lines generated using the β-estradiol MIKC^{C}-type MADS-box gene induction system. a, Gametangia in over-expression lines of each inducible MIKC^{C}-type MADS-box gene cultured with or without β-estradiol. **b**-**g**, Gametangia in PPM2 over-expression line cultured with β-estradiol. **c**,**e**,**g**, Magnified images of **b**,**d**, and **f**, respectively. Arrows indicate brown inner part (**b**), expanded cells (**c**,**e**), and elongated cells (**f**,**g**). Scale bars, 100 μm in **a**; 50 μm in **b**-**g**.

similar to *PPM2* (Fig. 26a). Furthermore, in *PPM2*- or *PPMC6*-induced lines, no archegonia were found at observation time when one or several archegonia develop in wild type and sperms were not observed in browned antheridia.

5. Discussion

Protein localization and functional analyses of Physcomitrella MIKC^{C}-type MADS-box genes revealed their roles in the gametophore stem and antheridia. The former is the negative regulation of the length of the gametophore internodes, which influences external water conductions (Fig. 18) necessary for sperm swimming to the egg (Fig. 21). The latter is the formation of motile sperm flagella (Fig. 22). These functions are both necessary for fertilization.

The internode length is determined by cell number and length, which are regulated by cell divisions and growth, respectively. Experiment data indicate that MIKC^{C}-type MADS-box genes are involved in the repression of both cell divisions and growth to maintain the gametophore internodes in the length appropriate for the external water conductions (Fig. 14). The external water conduction also functions to supply water to the surface of the gametophore, which otherwise easily dries out because the gametophore leaves comprise a single cell layer and the stem comprises only a few-cell thickness. In fact, when the sextuple deletion mutant gametophores, of which the surface looked dry, were moved to dry conditions (around 50% relative humidity; Fig. 27b), after 7 days the leaves shrank by drying, while those of the wild type, which have water on the surface, did not dry out after 7 days in dry conditions (Fig. 27a). Furthermore, when the wild-type gametophores cultured in no irrigation conditions, of which the surface looked dry, were moved to dry conditions, the gametophore leaves shrank similar to the sextuple deletion mutant line (Fig. 27a). These results indicate that external water conduction regulated by MIKC^{C}-type MADS-box genes is necessary for protecting gametophore leaves from drying.

In terms of flagellum movement, the expression levels of 23 putative

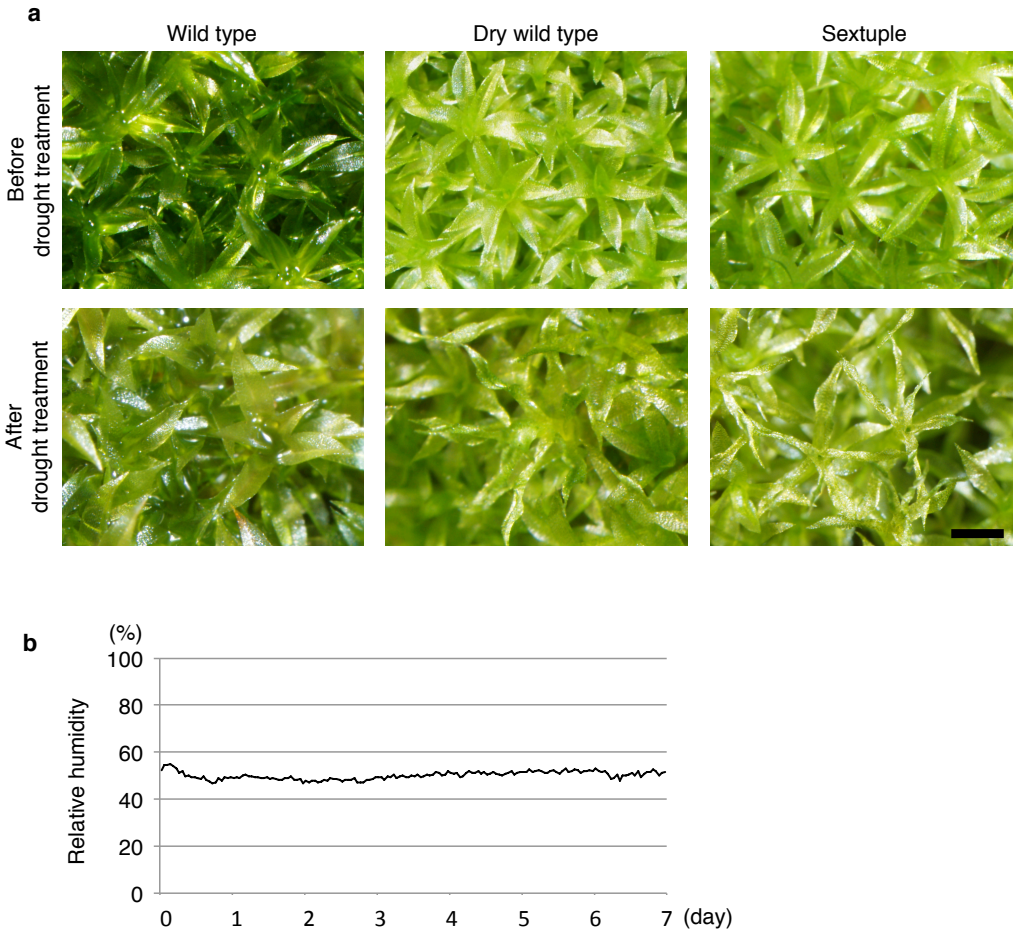

Figure 27 | Examination of effects by drought treatment. a, Gametophores before and after drought treatment in the wild type, dry wild type, which is not wet wild type cultured in no irrigation conditions, and sextuple deletion mutant line #109. **b,** Relative humidity during drought treatment for 7 days. Scale bar ; 2 mm in **a**.

orthologs of Chlamydomonas flagellum-related genes (Pazour et al., 2005) decreased in the antheridia of the sextuple and triple mutants compared to the wild type (Table 3). Seven out of the 23 flagellum-related genes encode dynein heavy chains, which are central pair apparatus proteins and components of dynein regulatory complex. Dynein regulatory complex regulates the flagella motility and bending in both Chlamydomonas and animals (Inaba, 2011). These results suggest that MIKC^{C}-type MADS-box genes are involved in flagellum motility through the regulation of flagellum-related genes including dynein heavy chain genes in Physcomitrella. However, visible alterations were not detected in the flagellum structures of the mutant, which were previously observed in sperms defective in flagellum movement using TEM in Chlamydomonas (Gardner et al., 1994) and mouse (Neesen et al., 2001; Zhang et al., 2006). Higher resolution microscopy including cryo-electron tomography (Nicastro et al., 2006) could be necessary to reveal the structural defects in the sperm flagella of the sextuple deletion mutant line, although the sperm number we can collect is not enough for such method. Once the method for massive sperm collection is established, one can analyse the structure in higher resolution with cryo-electron tomography to find the defects in the sperm flagella. As other possibility, flagellated plant sperms have a spline consisted of parallel microtubules along an elongated sperm nucleus, and the spline may contribute rotation movement of the sperm body. In this case, the defects of sperm movement in the deletion mutant lines are possibly caused by defects in spline.

Each MIKC^{C}-type MADS-domain protein localized in a different but partially overlapping pattern throughout the lifecycle of Physcomitrella (Figs. 10 and 11), and at least one MIKC^{C}-type MADS-domain protein localized in most cells. However, phenotypes of the sextuple deletion mutant lines were detected in only the gametophore

stems and sperms formed in antheridia (Figs. 14 and 22), where *PPM1*, *PPM2*, and *PPMC6* were co-localized (Fig. 10). Furthermore, the phenotypes detected in the sextuple deletion mutant lines were also observed in the triple deletion mutant lines of *PPM1*, *PPM2*, and *PPMC6* (Figs. 14 and 22), and over-expression of those three genes affected the gametophore stem and antheridia formation, but that of other three genes did not exhibit any obvious phenotype (Fig. 26). In addition, each *ppm1 ppm2*, *ppm1 ppmc6*, and *ppm2 ppmc6* double deletion mutant line showed phenotypes intermediate between the wild type and the triple deletion mutant line. These results indicate that *PPM1*, *PPM2*, and *PPMC6* play redundant roles in the gametophore stem and antheridia, and phenotypes observed in the sextuple deletion mutant lines are likely caused by the lesion of these three genes.

PPM1, *PPM2*, and *PPMC6* showed similar protein localization patterns and appeared to have redundant roles. Protein localization patterns of *PpMADS1*, *PPMC5*, and *PpMADS-S* were different from *PPM1*, *PPM2*, and *PPMC6* and also different from each other. *PPM1* and *PPM2* are the same clade but *PPMC6* is an another clade in the phylogenic tree of all six MIKC^{C}-type MADS-box genes (Fig. 9; Gramzow et al., 2012), therefore functions of *PPM1*, *PPM2*, and *PPMC6* in the gametophore stem and sperms are likely to be one of the ancestral functions of MIKC^{C}-type MADS-box genes before their divergence in the Physcomitrella lineage. Both single deletion mutant and ectopic expression lines of *PpMADS1*, *PPMC5*, and *PpMADS-S* were indistinguishable from the wild type, suggesting two hypotheses: These genes lost their function during the evolution or do not have conspicuous functions under the controlled laboratory conditions. In regard to the former hypothesis, genes with no function become pserudogenes during the evolution (Lynch and Conery, 2000). However, *PpMADS1*,

PPMC5, and *PpMADS-S* have clear open reading flame and gene expression (see Phytozome; https://phytozome.jgi.doe.gov/pz/portal.html). Expression patterns of *PPM2* were different between two previous studies (Singer et al., 2007; Quodt et al., 2007), suggesting that *PPM2* expression is regulated by unknown environmental or endogenous parameters (Quodt et al., 2007). *PpMADS1*, *PPMC5*, and *PpMADS-S* may also exhibit different expression patterns or conspicuous functions in environmental conditions, which was not examined in this research.

6. General discussion

These analyses showed that Physcomitrella MIKC^{C}-type MADS-box genes redundantly function in two ways to enable fertilization. One is to regulate the cell division and growth in gametophore stems, which results in appropriate internode length for external water conduction with capillarity. The other is to form motile sperms through regulating flagellum-related genes.

In regard to the growth regulation, several MIKC^{C}-type MADS-box genes function in organ growth in the late stages of flower development in angiosperms (Dornelas et al., 2011; Ito, 2011). In addition, one of the MIKC^{C}-type MADS-box genes in Arabidopsis, *XAANTAL1* (*XAL1*), regulates cell proliferation in the root meristem: *xal1* mutants show shortened meristem with a lower rate of cell proliferation and longer cell-cycle duration than in the wild type (Tapia-López et al., 2008). In addition, over-expression of Arabidopsis *SOC1* and *AGAMOUS-LIKE 24* (*AGL24*) genes results in elongated carpels (Borner et al., 2000; Michaels et al., 2003). Furthermore, MIKC^{C}-type MADS-box genes in the gymnosperms *Picea abies*, *Picea glauca*, and *Pinus taeda* are expressed in roots and shoot apices (Gramzow et al., 2014), which have high cell division activity. In the monilophyte *Ceratopteris richardii*, MIKC^{C}-type MADS-box genes are expressed in tissues with high activities of cell division, and their involvement in organ growth has been suggested (Hasebe et al., 1998). The function of MIKC^{C}-type MADS-box genes in growth regulation is similar between vascular plants and Physcomitrella, and the growth regulation is most likely one of the ancient functions of MIKC^{C}-type MADS-box genes in land plants.

In the aspect of the motile flagella formation, MIKC^{C}-type MADS-box gene in the charophycean green algae *Chara globularis* is expressed during flagellate sperm

differentiation. This suggests that the regulation of the flagellum-related genes by MIKC^{C}-type MADS-box proteins dates back to the common ancestor of the charophycean green algae and land plants. In addition, MIKC^{C}-type MADS-box genes in ferns *C. richardii* and *D. fragrans* are expressed in gametophytes with antheridia (Hasebe et al., 1998; Huang et al., 2014). Therefore, MIKC^{C}-type MADS-box genes may also function in the motile flagella formation in the fern lineage. On the other hand, sperms with motile flagella was lost during the evolution of angiosperms. Accordingly, orthologs of nine flagellum-related genes including genes encoding dynein motor proteins regulated by Physcomitrella MIKC^{C}-type MADS-box genes were not found in the Arabidopsis genome (Table 3). This suggests that they were lost during the evolutionary transition from the use of flagellate sperm to pollen tubes for fertilization. Orthologs of other 14 flagellum-related genes exist and likely function in other processes in Arabidopsis.

These results give insights into both the commonality and diversity of the MADS-box genes throughout land plant evolution. MADS-box genes are involved in growth regulation in both Physcomitrella and the flowering plants, suggesting that the MIKC^{C}-type MADS-box genes of the common ancestor of land plants also had such function. By contrast, the regulation of flagellum-related genes was lost in the flowering plant lineage in accordance with the loss of sperm. This study also shows that the most conspicuous functions of MIKC^{C}-type MADS-box genes as homeotic selectors in floral organ development evolved in the vascular plant lineage in accord with the evolution of flowers after the divergence of the mosses. Functions as homeotic selectors in floral organ development require interaction and complex formation between different MIKC^{C}-type MADS-domain proteins (Smaczniak et al., 2012a). In this study, the

interactions between MIKC^C-type MADS-box proteins were not examined. However, it is unlikely in Physcomitrella that complex formation between different types of MIKC^C-type MADS-domain proteins is necessary for their functions, because the single deletion mutant lines were indistinguishable from the wild type (Fig. 13). *PPM1*, *PPM2*, and *PPMC6* had redundant roles, indicating that *PPM1*, *PPM2*, and *PPMC6* function as the same type of MADS-box gene. If *PPM1*, *PPM2*, and *PPMC6* interact each other, homo- and heterocomplex must have same role. Structures of I, K, and C domains for complex formation are conserved in Physcomitrella and also in green algae, which have single MIKC^C-type MADS-box gene (Tanabe et al., 2005). This suggests that MIKC^C-type MADS-domain protein had the ability of homocomplex formation in the common ancestor of green plants, and then acquired the ability of heterocomplex formation between different types of MIKC^C-type MADS-domain proteins in accord with gene/genome duplication followed by sub-/neo-functionalization. On the other hand, Physcomitrella MIKC^C-type MADS-domain proteins were expressed differently in band patterns in developing sporophytes (Fig. 10). This may suggest that Physcomitrella MIKC^C-type MADS-box genes repress each other like A- and C-function genes in flower formation in angiosperms (Ma, 1994). Future analyses of functions, regulations, and interactions of MIKC^C-type MADS-box genes in land plants outside of angiosperms will give us more insights regarding the evolution of MIKC^C-type MADS-box genes as homeotic selectors of floral organ identity.

7. Acknowledgements

I am deeply indebted to Professor Mitsuyasu Hasebe for his generous supports, advice, and helpful discussion. I am grateful to Associate professor Takashi Murata for helpful discussion, guidance, and experiment support for my project. I am also grateful to Dr. Yosuke Tamada for helpful discussion. I sincerely wish to thank Dr. Naoki Aono, for his research as a basis of my project. This work would have not been possible without their understanding and supports.

I would like to thank the collaborators, Dr. Rumiko Kofuji for initial experiments of my project and discussion, Drs. Yuko Sasaki-Sekimoto, Mie Shimojima, and Hiroyuki Ohta for their excellent work of wax analyses and discussion, Dr. Masahide Kikkawa for sperm analyses and discussion, Dr. Shuji Shigenobu for transcriptome analyses, and Drs. Yukiko Kabeya and Yuji Hiwatashi for producing transgenic lines and technical supports.

I also would like to thank Drs. Tomoaki Nishiyama, Keiko Sakakibara, and Yoichi Sakata for discussion, the members of the Division of Evolutionary Biology for discussion and supports, and Dr. Taro Maeda for advice on the transcriptome analyses. I also thank Model Plant Research Facility, Spectrography and Bioimaging Facility, and Data Integration and Analysis Facility in National Institute for Basic Biology, and EM facility in National Institute for Physiological Sciences for their technical supports.

Finally, I thank my family and friends for many supports.

8. References

Barker, E.I. and Ashton, N.W. (2013). A parsimonious model of lineage-specific expansion of MADS-box genes in *Physcomitrella patens*. Plant Cell Rep. **32**: 1161–1177.

Becker, A., Winter, K.U., Meyer, B., Saedler, H., and Theissen, G. (2000). MADS-box gene diversity in seed plants 300 million years ago. Mol. Biol. Evol. **17**: 1425–1434.

Beike, A.K., Stackelberg, V.M., Schallenberg-rüdinger, M., Hanke, S.T., and Follo, M. (2014). Molecular evidence for convergent evolution and allopolyploid speciation within the Physcomitrium - Physcomitrella species complex. BMC Evol. Biol. **14**: 1–19.

De Bodt, S., Raes, J., Florquin, K., Rombauts, S., Rouzé, P., Theißen, G., and Van De Peer, Y. (2003). Genomewide structural annotation and evolutionary analysis of the type I MADS-box genes in plants. J. Mol. Evol. **56**: 573–586.

Borner, R., Kampmann, G., Chandler, J., Gleißner, R., Wisman, E., Apel, K., and Melzer, S. (2000). A MADS domain gene involved in the transition to flowering in Arabidopsis. Plant J. **24**: 591–599.

Buda, G.J., Barnes, W.J., Fich, E.A., Park, S., Yeats, T.H., Zhao, L., Domozych, D.S., and Rose, J.K.C. (2013). An ATP binding cassette transporter is required for cuticular wax deposition and desiccation tolerance in the moss *Physcomitrella patens*. Plant Cell **25**: 4000–13.

Budke, J.M., Goffinet, B., and Jones, C.S. (2011). A hundred-year-old question: is the moss calyptra covered by a cuticle? A case study of *Funaria hygrometrica*. Ann. Bot. **107**: 1279–1286.

Dornelas, M.C., Patreze, C.M., Angenent, G.C., and Immink, R.G.H. (2011). MADS: the missing link between identity and growth? Trends Plant Sci. **16**: 89–97.

Fluhr, R., Moses, P., Morelli, G., Coruzzi, G., and Chua, N.H. (1986). Expression dynamics of the pea rbcS multigene family and organ distribution of the transcripts. EMBO J. **5**: 2063–2071.

Gardner, L.C., O'Toole, E., Perrone, C.A., Giddings, T., and Porter, M.E. (1994). Components of a "dynein regulatory complex" are located at the junction between the radial spokes and the dynein arms in Chlamydomonas Flagella. J. Cell Biol. **127**: 1311–1325.

Gramzow, L., Barker, E., Schulz, C., Ambrose, B., Ashton, N., Theißen, G., and

Litt, A. (2012). Selaginella genome analysis – entering the "homoplasy heaven" of the MADS world. Front. Plant Sci. **3**: 1–14.

Gramzow, L. and Theissen, G. (2010). A hitchhiker's guide to the MADS world of plants. Genome Biol. **11**: 214–225.

Gramzow, L., Weilandt, L., and Theißen, G. (2014). MADS goes genomic in conifers: towards determining the ancestral set of MADS-box genes in seed plants. Ann. Bot. **114**: 1407–1429.

Greer, S., Wen, M., Bird, D., Wu, X., Samuels, L., Kunst, L., and Jetter, R. (2007). The cytochrome P450 enzyme CYP96A15 is the midchain alkane hydroxylase responsible for formation of secondary alcohols and ketones in stem cuticular wax of Arabidopsis. Plant Physiol. **145**: 653–667.

Gregis, V. et al. (2013). Identification of pathways directly regulated by SHORT VEGETATIVE PHASE during vegetative and reproductive development in Arabidopsis. Genome Biol. **14**: 1–26.

Griesbeck, O., Baird, G.S., Campbell, R.E., Zacharias, D.A., and Tsien, R.Y. (2001). Reducing the environmental sensitivity of yellow fluorescent protein. J. Biol. Chem. **276**: 29188–29194.

Harrison, C.J. (2017). Development and genetics in the evolution of land plant body plans. Phil. Trans. R. Soc. Lond. B. **372**: 1–12.

Hasebe, M., Wen, C.K., Kato, M., and Banks, J.A. (1998). Characterization of MADS homeotic genes in the fern *Ceratopteris richardii*. Proc. Natl. Acad. Sci. USA **95**: 6222–6227.

Henschel, K., Kofuji, R., Hasebe, M., Saedler, H., Münster, T., and Theissen, G. (2002). Two ancient classes of MIKC-type MADS-box genes are present in the moss *Physcomitrella patens*. Mol. Biol. Evol. **19**: 801–814.

Himi, S., Sano, R., Nishiyama, T., Tanahashi, T., Kato, M., Ueda, K., and Hasebe, M. (2001). Evolution of MADS-box gene induction by FLO/LFY genes. J. Mol. Evol. **53**: 387–393.

Hiwatashi, Y., Obara, M., Sato, Y., Fujita, T., Murata, T., and Hasebe, M. (2008). Kinesins are indispensable for interdigitation of phragmoplast microtubules in the moss *Physcomitrella patens*. Plant Cell **20**: 3094–3106.

Hohe, A., Rensing, S.A., Mildner, M., Lang, D., and Reski, R. (2002). Day length and temperature strongly influence sexual reproduction and expression of a novel MADS-box gene in the moss *Physcomitrella patens*. Plant Biol. **4**: 595–602.

Huang, Q., Li, W., Fan, R., and Chang, Y. (2014). New MADS-box gene in fern: cloning and expression analysis of DfMADS1 from *Dryopteris fragrans*. PLoS

One **9**: 1–6.

Imaizumi, T., Kadota, A., Hasebe, M., and Wada, M. (2002). Cryptochrome light signals control development to suppress auxin sensitivity in the moss *Physcomitrella patens*. Plant Cell **14**: 373–386.

Inaba, K. (2011). Sperm flagella : comparative and phylogenetic perspectives of protein components. Mol. Hum. Reprod. **17**: 524–538.

Ishikawa, M. et al. (2011). Physcomitrella cyclin-dependent kinase a links cell cycle reactivation to other cellular changes during reprogramming of leaf cells. Plant Cell **23**: 2924–38.

Ito, T. (2011). Coordination of flower development by homeotic master regulators. Curr. Opin. Plant Biol. **14**: 53–59.

Jefferson, R.A. (1987). Assaying chimaeric genes in plants : the GUS gene fusion system. Plant Mol. Biol. Rep. **5**: 387–405.

Kamiya, R. and Witman, G.B. (1984). Submicromolar levels of calcium control the balance of beating between the two flagella in demembranated models of Chlamydomonas. J. Cell Biol. **98**: 97–107.

Kaufmann, K., Melzer, R., and Theißen, G. (2005). MIKC-type MADS-domain proteins: structural modularity, protein interactions and network evolution in land plants. Gene **347**: 183–198.

Kaufmann, K., Wellmer, F., Muiño, J.M., Ferrier, T., Wuest, S.E., Kumar, V., Serrano-mislata, A., Madueño, F., Krajewski, P., Meyerowitz, E.M., Angenent, G.C., and Riechmann, J.L. (2010). Orchestration of floral initiation by APETALA1. Science **328**: 85–90.

Kofuji, R., Sumikawa, N., Yamasaki, M., Kondo, K., Ueda, K., Ito, M., and Hasebe, M. (2003). Evolution and divergence of the MADS-box gene family based on genome-wide expression analyses. Mol. Biol. Evol. **20**: 1963–1977.

Kondo, S., Hori, K., Sasaki-Sekimoto, Y., Kobayashi, A., Kato, T., Yuno-Ohta, N., Nobusawa, T., Ohtaka, K., Shimojima, M., and Ohta, H. (2016). Primitive extracellular lipid components on the surface of the charophytic alga *Klebsormidium flaccidum* and their possible biosynthetic pathways as deduced from the genome sequence. Front. Plant Sci. **7**: 1–15.

Kubo, M., Imai, A., Nishiyama, T., Ishikawa, M., Sato, Y., Kurata, T., Hiwatashi, Y., Reski, R., and Hasebe, M. (2013). System for stable β-estradiol-inducible gene expression in the moss *Physcomitrella patens*. PLoS One **8**: 1–13.

Kwantes, M., Liebsch, D., and Verelst, W. (2012). How MIKC * MADS-box genes originated and evidence for their conserved function throughout the evolution of

vascular plant gametophytes. Mol. Biol. Evol. **29**: 293–302.

Landberg, K., Pederson, E.R.A, Viaene, T., Bozorg, B., Friml, J., Jönsson, H., Thelander, M., and Sundberg, E. (2013). The moss *Physcomitrella patens* reproductive organ development is highly organized, affected by the two SHI/STY genes and by the level of active auxin in the SHI/STY expression domain. Plant Physiol. **162**: 1406–19.

Larkin, M.A. et al. (2007). Clustal W and Clustal X version 2.0. Bioinformatics **23**: 2947–2948.

Li-beisson, Y. et al. (2013). Acyl-lipid metabolism. The Arabidopsis Book **e0161**: 1–70.

Lynch, M. and Conery, J.S. (2000). The evolutionary fate and consequences of duplicate genes. Science **290**: 1151–1156.

Ma, H. (1994). The unfolding drama of flower development : recent results from genetic and molecular analyses. Genes Dev. **8**: 745–756.

Maoiléidigh, D.S.Ó., Wuest, S.E., Rae, L., Raganelli, A., Ryan, P.T., Das, P., Lohan, A.J., Loftus, B., Graciet, E., and Kwa, K. (2013). Control of reproductive floral organ identity specification in Arabidopsis by the C function regulator AGAMOUS. Plant Cell **25**: 2482–2503.

Michaels, S.D., Ditta, G., Gustafson-Brown, C., Pelaz, S., Yanofsky, M., and Amasino, R.M. (2003). AGL24 acts as a promoter of flowering in Arabidopsis and is positively regulated by vernalization. Plant J. **33**: 867–874.

Miyamura, S., Matsunaga, S., and Hori, T. (2002). High-speed video microscopical analysis of the flagellar movement of *Marchantia polymorpha* sperm. Bryol. Res. **8**: 79–83.

Münster, T., Pahnke, J., Rosa, A. Di, Kim, J.T., Martin, W., Saedler, H., and Theissen, G. (1997). Floral homeotic genes were recruited from homologous MADS-box genes preexisting in the common ancestor of ferns and seed plants. Proc. Natl. Acad. Sci. USA **94**: 2415–2420.

Neesen, J., Kirschner, R., Ochs, M., Schmiedl, A., Habermann, B., Mueller, C., Holstein, A.F., Nuesslein, T., Adham, I., and Engel, W. (2001). Disruption of an inner arm dynein heavy chain gene results in asthenozoospermia and reduced ciliary beat frequency. Hum. Mol. Genet. **10**: 1117–28.

Nicastro, D., Schwartz, C., Pierson, J., Gaudette, R., Porter, M.E., and Mcintosh, J.R. (2006). The molecular architecture of axonemes revealed by cryoelectron tomography. Science **313**.

Nishiyama, T., Hiwatashi, Y., Sakakibara, K., Kato, M., and Hasebe, M. (2000).

Tagged mutagenesis and gene-trap in the moss, *Physcomitrella patens* by shuttle mutagenesis. DNA Res. **7**: 9–18.

Ohara, A., Kato-minoura, T., Kamiya, R., and Hirono, M. (1998). Recovery of flagellar inner-arm dynein and the fertilization tubule in Chlamydomonas ida5 mutant by transformation with actin genes. Cell Struct. Funct. **281**: 273–281.

Okano, Y., Aono, N., Hiwatashi, Y., Murata, T., Nishiyama, T., Ishikawa, T., Kubo, M., and Hasebe, M. (2009). A polycomb repressive complex 2 gene regulates apogamy and gives evolutionary insights into early land plant evolution. Proc. Natl. Acad. Sci. USA **106**: 16321–16326.

Parenicova, L. (2003). Molecular and phylogenetic analyses of the complete MADS-box transcription factor family in Arabidopsis: new openings to the MADS world. Plant Cell **15**: 1538–1551.

Pazour, G.J., Agrin, N., Leszyk, J., and Witman, G.B. (2005). Proteomic analysis of a eukaryotic cilium. J. Cell Biol. **170**: 103–113.

Proctor, M.C.F. (2008). Bryophyte Biology: Second Edition: Physiological ecology B. Goffinet and A.J. Shaw, eds (Cambridge University Press).

Quodt, V., Faigl, W., Saedler, H., and Münster, T. (2007). The MADS-domain protein PPM2 preferentially occurs in gametangia and sporophytes of the moss *Physcomitrella patens*. Gene **400**: 25–34.

Rensing, S.A. et al. (2008). The Physcomitrella genome reveals evolutionary insights into the conquest of land by plants. Science **319**: 64–69.

Riechmann, J.L., Krizek, B.A., and Meyerowitz, E.M. (1996). Dimerization specificity of Arabidopsis MADS domain homeotic proteins APETALA1, APETALA3, PISTILLATA, and AGAMOUS. Proc. Natl. Acad. Sci. USA **93**: 4793–4798.

Sakakibara, K., Nishiyama, T., Deguchi, H., and Hasebe, M. (2008). Class 1 KNOX genes are not involved in shoot development in the moss *Physcomitrella patens* but do function in sporophyte development. Evol. Dev. **10**: 555–566.

Sasagawa, Y., Nikaido, I., Hayashi, T., Danno, H., Uno, K.D., Imai, T., and Ueda, H.R. (2013). Quartz-Seq: a highly reproducible and sensitive single-cell RNA-Seq reveals non-genetic gene expression heterogeneity. Genome Biol. **14**: 1–17.

Schwarz-sommer, Z., Huijser, P., and Nacgen, W. (1990). Genetic control of flower development by homeotic genes in *Antirrhinum majus*. Science **250**: 931–936.

Seo, E., Lee, H., Jeon, J., Park, H., Kim, J., Noh, Y.-S., and Lee, I. (2009). Crosstalk between cold response and flowering in Arabidopsis is mediated through the flowering-time gene SOC1 and its upstream negative regulator FLC. Plant Cell **21**:

3185–3197.

Shindo, S., Ito, M., Ueda, K., Kato, M., and Hasebe, M. (1999). Characterization of MADS genes in the gymnosperm *Gnetum parvifolium* and its implication on the evolution of reproductive organs in seed plants. Evol. Dev. **1**: 180–90.

Singer, S.D., Krogan, N.T., and Ashton, N.W. (2007). Clues about the ancestral roles of plant MADS-box genes from a functional analysis of moss homologues. Plant Cell Rep. **26**: 1155–1169.

Smaczniak, C., Immink, R.G.H., Angenent, G.C., and Kaufmann, K. (2012a). Developmental and evolutionary diversity of plant MADS-domain factors: insights from recent studies. Development **139**: 3081–3098.

Smaczniak, C., Immink, R.G.H., Muiño, J.M., Blanvillain, R., and Busscher, M. (2012b). Characterization of MADS-domain transcription factor complexes in Arabidopsis flower development. Proc. Natl. Acad. Sci. USA **109**: 1560–1565.

Sun, J., Nishiyama, T., Shimizu, K., and Kadota, K. (2013). TCC: an R package for comparing tag count data with robust normalization strategies. BMC Bioinformatics **14**: 1–13.

Tanabe, Y., Hasebe, M., Sekimoto, H., Nishiyama, T., Kitani, M., Henschel, K., Munster, T., Theissen, G., Nozaki, H., and Ito, M. (2005). Characterization of MADS-box genes in charophycean green algae and its implication for the evolution of MADS-box genes. Proc. Natl. Acad. Sci. USA **102**: 2436–2441.

Tanahashi, T., Sumikawa, N., Kato, M., and Hasebe, M. (2005). Diversification of gene function: homologs of the floral regulator FLO/LFY control the first zygotic cell division in the moss *Physcomitrella patens*. Development **132**: 1727–1736.

Tao, Z., Shen, L., Liu, C., Liu, L., Yan, Y., and Yu, H. (2012). Genome-wide identification of SOC1 and SVP targets during the floral transition in Arabidopsis. Plant J. **70**: 549–561.

Tapia-López, R., García-Ponce, B., Dubrovsky, J.G., Garay-Arroyo, A., Pérez-Ruíz, R. V, Kim, S.-H., Acevedo, F., Pelaz, S., and Alvarez-Buylla, E.R. (2008). An AGAMOUS-related MADS-box gene, XAL1 (AGL12), regulates root meristem cell proliferation and flowering transition in Arabidopsis. Plant Physiol. **146**: 1182–92.

Waterhouse, A.M., Procter, J.B., Martin, D.M.A., Clamp, M., and Barton, G.J. (2009). Jalview Version 2-a multiple sequence alignment editor and analysis workbench. Bioinformatics **25**: 1189–1191.

Wickett, N.J. et al. (2014). Phylotranscriptomic analysis of the origin and early diversification of land plants. Proc. Natl. Acad. Sci. USA **111**: E4859–E4868.

Wu, M., Sang, Y., Bezhani, S., Yamaguchi, N., Han, S., Li, Z., and Su, Y. (2012). SWI2/SNF2 chromatin remodeling ATPases overcome polycomb repression and control floral organ identity with the LEAFY and SEPALLATA3 transcription factors. Proc. Natl. Acad. Sci. USA **109**: 3576–3581.

Wuest, S.E., Maoileidigh, D.S.O., Rae, L., Kwasniewska, K., Raganelli, A., Hanczaryk, K., Lohan, A.J., Loftus, B., Graciet, E., and Wellmer, F. (2012). Molecular basis for the specification of floral organs by APETALA3 and PISTILLATA. Phil. Trans. R. Soc. Lond. B. **109**: 13452–13457.

Yanofsky, M.F., Ma, H., Bowman, J.L., Drews, G.N., Feldmann, K.A., and Meyerowitz, E.M. (1990). The protein encoded by the Arabidopsis homeotic gene agamous resembles transcription factors. Nature **346**: 35–39.

Zhang, Z., Kostetskii, I., Tang, W., Haig-Ladewig, L., Sapiro, R., and Wei, Z. (2006). Deficiency of SPAG16L causes male infertility associated with impaired sperm motility. Biol. Reprod. **74**: 751–759.

Zuo, J., Niu, Q.W., and Chua, N.H. (2000). An estrogen receptor-based transactivator XVE mediates highly inducible gene expression in transgenic plants. Plant J. **24**: 265–273.